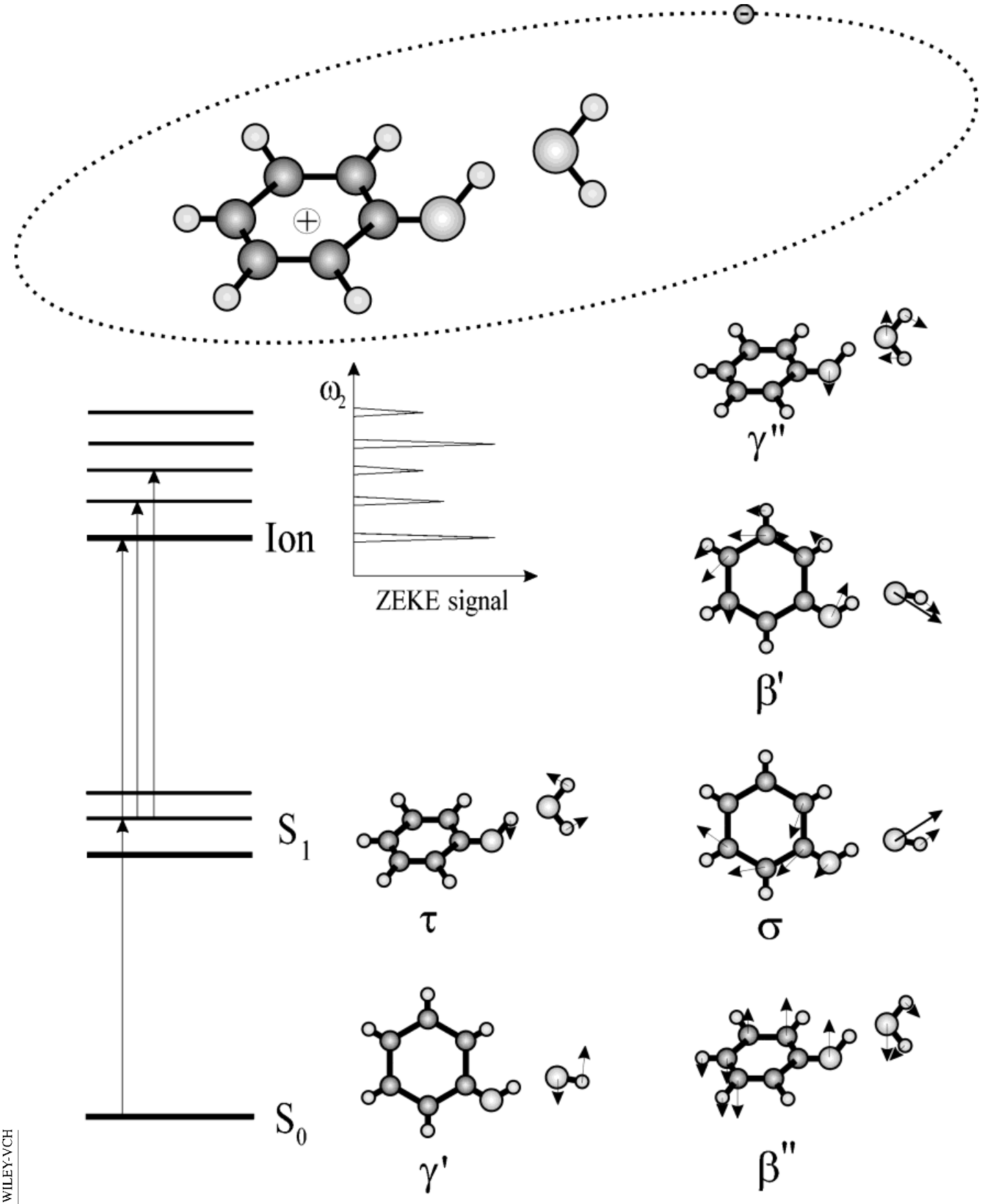

ZEKE spectroscopy shows for the first time the intermolecular vibrational modes of the phenol–water cation.

Chemical Applications of Zero Kinetic Energy (ZEKE) Photoelectron Spectroscopy

Klaus Müller-Dethlefs* and Edward W. Schlag

ZEKE spectroscopy is a new method in chemical spectroscopy which particularly addresses ionic species by measuring (ro)vibronic states of the ion through detection of isoenergetic, stable Rydberg states. These states are extremely long-lived and can therefore be measured with high precision. The new spectroscopy allows very high resolution measurements of positively charged ions. This approach can be extended to photodetachment of anions, producing information about the corresponding neutral molecule. ZEKE spectroscopy has already been applied to a wide variety of molecular ions, clusters, van der Waals molecules, free radicals, reactive intermediates, and even to elusive transition states of chemical reactions. Compared to conventional photoelectron spectroscopy, ZEKE spectroscopy offers many advantages, for example, greatly increased spectral resolution. This allows one to obtain the rotational structure of large molecular cations such as the benzene cation and the intermolecular vibrations of molecular clusters such as phenol – water.

Keywords: cations · clusters · photoelectron spectroscopy · Rydberg states · ZEKE spectroscopy

1. Introduction

Spectroscopic techniques such as NMR, IR, or UV/Vis spectroscopy have been crucial for the understanding of the structure and reactivity of molecules.[1] There remain, however, a plethora of chemical systems—for example, ions, van der Waals complexes, and reactive intermediates—which are difficult if not impossible to probe by these traditional approaches. This review presents the application of a relatively new spectroscopic method, ZEKE spectroscopy (*ze*ro *k*inetic *e*nergy photoelectron spectroscopy), to such species to further our understanding of the structures of complex chemical systems.

ZEKE spectroscopy is an evolution of the well-known photoionization technique developed in the 1960s, photoelectron spectroscopy (PES).[2–4] Photoionization can be described as the removal of an electron from the HOMO (*h*ighest *o*ccupied *m*olecular *o*rbital) into the ionization continuum, thus creating a molecular cation in its electronic ground state. Furthermore, removal of an electron from an orbital below the HOMO (with higher ionization energy E_i) will produce an excited electronic state of the cation. A photoelectron spectrum of benzene obtained with vacuum UV (VUV) radiation is presented in Figure 1 (together with the frontier molecular orbitals); the bands can be assigned to the ground state and electronically excited states of the benzene cation. PES provides quantitative information about the electronic and vibronic states of molecular ions[4–6] through analysis of the kinetic energy of the ejected photoelectrons. The molecule to be analyzed is irradiated with monoenergetic photons that ionize the molecule, and any excess energy is transformed into kinetic energy of the electron [Eq. (a); n, S, v, and N represent electronic, electronic-spin, vibrational, and rotational quantum numbers, E_i is the ionization energy, and $E_{kin}(e^-)$ is the kinetic energy of the electron]. Partially

$$E^{int}_{neutral}(n, S, v, N) + h\nu - E_i \rightarrow E^{int}_{ion}(n^+, S^+, v^+, N^+) + E_{kin}(e^-) \quad \text{(a)}$$

resolved fine structure is visible in the VUV photoelectron spectrum of benzene, and corresponds to rotationally and vibrationally excited levels of the cation which are populated in accordance with Equation (a). As a zero-order approximation (in which electron correlation is ignored), the ionization energies can be equated to the negative orbital energies following Koopmans theorem. Though rarely accurate in practice, Koopmans theorem has proven conceptually that molecular orbitals are more than just a product of the quantum chemist's imagination and has contributed to the understanding of the electronic structure of molecules.

[*] Prof. Dr. K. Müller-Dethlefs
Department of Chemistry
University of York
Heslington, York, YO1 5DD (UK)
Fax: (+44) 1904-434527
E-mail: kmd6@york.ac.uk
Prof. Dr. E. W. Schlag
Institut für Physikalische und Theoretische Chemie der Technischen Universität München, Garching (Germany)

  1433-7851/98/3710-1347 $ 17.50+.50/0

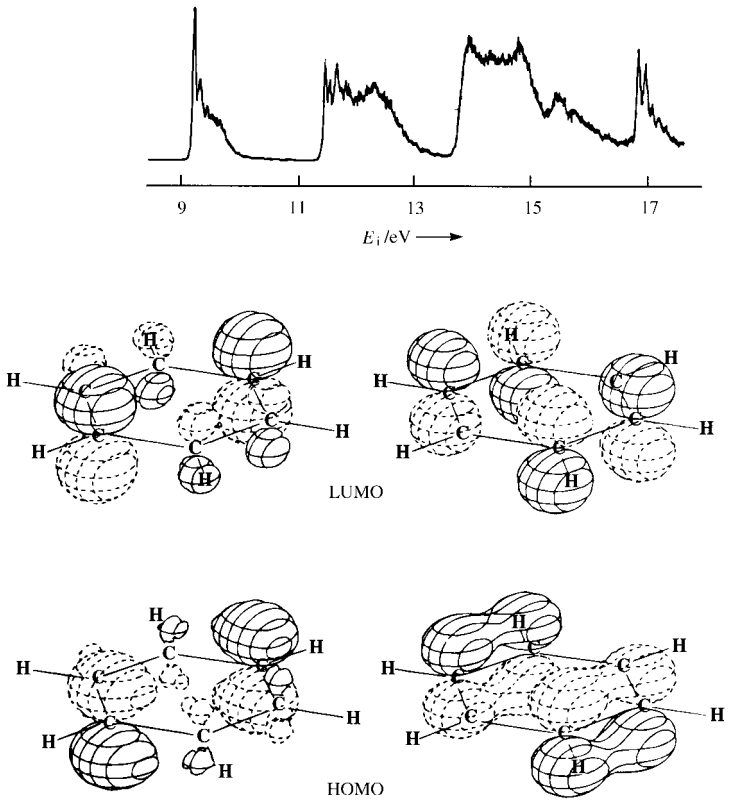

Figure 1. VUV photoelectron spectrum of benzene (top) and comparison of the frontier orbitals of benzene (bottom).[6]

While there is no fundamental limit to the resolution of PES, since the energy of the ejected electron is quantized (assuming sharp photon energy and molecular states of the cation and the neutral molecule), the practical resolution is limited by the necessity of determining the kinetic energy of the electrons. Firstly, calibration of the detector is necessary, and, secondly, the resolution of commercially available geometrical or time-of-flight (TOF) photoelectron analysers is generally limited to about 10 meV, although it can be improved to 3–5 meV with a combination of a He^I source and a spherical analyzer.[7] When combined with resonance enhanced multiphoton ionization (REMPI) a similar resolution was achieved in some cases.[8,9] With the notable exception of hydrogen[10–12] and some high-lying states of NO^+,[8,9] conventional PES is unable to resolve rotational states of ions. In addition, intermolecular vibrations in van der Waals clusters (whose frequency generally ranges between 10 and 400 cm^{-1}) cannot be elucidated with this approach.

The ZEKE method developed in our laboratory over the last decade overcomes the limitations of PES by producing electrons with no kinetic energy by matching the photon energy exactly to the energy for the transition from the state of the neutral molecule and that of the ion state.[13–22] This is achieved experimentally by scanning a laser or a VUV light

K. Müller-Dethlefs

E. W. Schlag

Klaus Müller-Dethlefs was born in 1950 in Wilster (Germany). After studying chemistry at the Universität Göttingen he received this Ph.D. in 1979 at Imperial College, University of London for his work on soot formation with F. Weinberg, supported by a bursary from the Evangelisches Studienwerk Villigst. With a research fellowship of the Deutsche Forschungsgemeinschaft, he worked with J. P. Taran at ONERA (Chatillon, France) on coherent anti-Stokes Raman spectroscopy (CARS) in flames. At the Institut für Physikalische und Theoretische Chemie der Technischen Universität München, he established the ZEKE spectroscopic method and its new applications in chemistry. Müller-Dethlefs was granted his habilitation in chemistry in 1991, and in 1994 he received the Rudolf-Kaiser-Preis of the Stiftungsverband für die Deutsche Wissenschaft in recognition of his development of ZEKE spectroscopy. He held guest professorships at the Université de Bourgogne (Dijon, France) in 1985 and at the Laboratoire Aimé Cotton (Orsay, France) in 1992. In 1995 he was appointed to the Chair of Physical Chemistry at the University of York. Presently, his main interests lie in the structure and dynamics of molecular ions, molecular clusters, and transient species as well as the study of proton and charge transfer with high resolution spectroscopic and time-resolved methods.

Edward W. Schlag was born in 1932 in Los Angeles (USA). He studied chemistry at Occidental College (Los Angeles), and received his Ph.D. at the University of Washington (Seattle) in 1958 under the supervision of B. S. Rabinovitch for work on the unimolecular isomerization of cyclopropanes. Since 1971 he has been a Professor for Physical Chemistry at the Technische Universität München. He has received several honors for his diverse research activities, which have been reported in more than 300 original papers and book contributions. He is a full member of the Bavarian Academy of Sciences, of Academia Europaea, and since 1984 a fellow of the Americal Physical Society. In 1988 he was made an honorary Doctor of the Hebrew University in Jerusalem. His main interests currenty focus on the investigation of the structure and dynamics of molecules and molecular complexes with high resolution spectroscopic methods and the laser mass spectrometry of large biomolecules.

source such as synchrotron radiation across an ionization threshold and selectively detecting electrons with zero kinetic energy. ZEKE spectroscopy has been extensively used by many other groups, making it impossible to present a representative cross-section of the present work. The reader is therefore directed to two recent books[19,153] and a review[21] for further references. The present review first describes an overview of the ZEKE method and then concentrates on a selection of chemical applications.

In contrast to conventional PES, ZEKE spectroscopy offers a resolution that is essentially limited by the typical bandwidth of a tunable pulsed dye laser (about 0.1 cm^{-1}).[17,23–25] This enables the resolution of rotational states of larger molecular cations and even the preparation of specific rovibronic states, opening the way to new experiments in chemical reaction dynamics. For molecular transitions between two bound states the selection rule $\Delta J = 0, \pm 1$ must be followed, whereas angular momentum transfers between the ion and molecule that are larger than ± 1 are possible for ionizing transitions. Especially rewarding is the combination of the ZEKE method with resonance enhanced multiphoton ionization (REMPI), where ionization occurs through one or more intermediate states. Owing to the Franck–Condon principle these intermediate states act as a kind of "filter" for the final state, thus further increasing the resolution. REMPI has been extremely successful as a sensitive method for obtaining electronic excitation spectra with rovibronic-state resolution. This has enabled the study of Rydberg-state dynamics,[15,26] photofragmentation processes, and the dynamics of photoionization apparent in the coupling between the molecular ion core (in a certain eigenstate) and the ejected photoelectron.[19,27]

A further significant improvement in resolution arises from the involvement of Rydberg states. If the photon energy falls just short of the ionization energy, an electron is promoted to a Rydberg state (a state with a high principal quantum number n). Whereas low-lying Rydberg states (with low n) readily interact with the molecular core and rapidly decay through radiationless transitions (i.e., predissociation or autoionization), the higher Rydberg states ($n > 150$) have lifetimes up to some ten microseconds and can be selectively ionized with pulsed-field ionization (PFI).[24,25,28] This "magic" Rydberg region (typically 1 meV below the ionization threshold) can be used to produce a ZEKE signal with high resolution. The term "magic" was applied to the Rydberg states that exist in this region because of to their unexpectedly long lifetimes.[29] Chupka[30] originally pointed out that this lengthening in lifetime probably arises due to mixing of the angular momentum l and its projection m_l, which results in a lifetime $\tau \propto n^5$ instead of the usual $\tau \propto n^3$.[31] ZEKE-PFI[28] has now become the most widespread experimental realization of ZEKE spectroscopy.

The superiority of the resolution (about three orders of magnitude) of the ZEKE method over traditional PES is illustrated in Figure 2. The vibrationally resolved photoelectron spectrum of NO, excited by a He^I light source,[4] is compared to the first ZEKE spectrum measured in 1984 with the $C^2\Pi$ state of NO as intermediate resonance in a (3+1) photoionization experiment.[14] In the ZEKE spectrum (Figure 2, bottom) the rotational structure of the NO^+ cation is fully resolved. Recent rotationally resolved ZEKE spectra of the benzene cation[32,53] were used to settle the debate regarding the structure of the ion, which is, in fact, planar and adequately described in the D_{6h} molecular point group, although it is subject to Jahn–Teller distortion.[1]

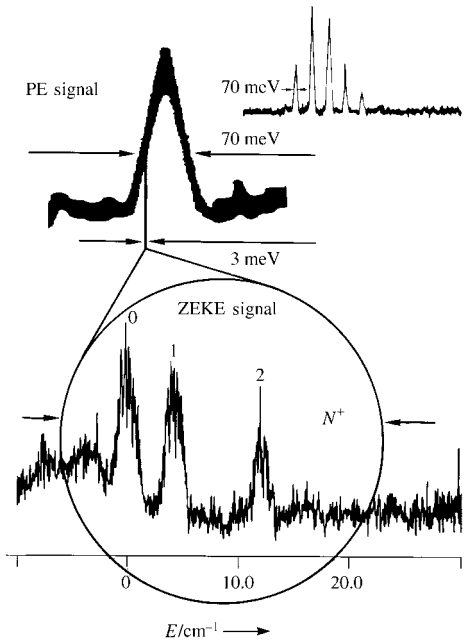

Figure 2. The first VUV photoelectron spectrum of NO[4] (top) with a vibrational progression from $v^+ = 0$ to $v^+ = 4$ of the $^1\Sigma^+$ electronic ground state of NO^+ and comparison of the $v^+ = 0$ peak with the first ZEKE spectrum obtained.[14] The ZEKE spectrum shows the lowest rotational states in the vibrational state $v^+ = 0$ with $N^+ = 0-2$.

In the field of vibrational spectroscopy the ZEKE method also achieves a major improvement over PES, as illustrated by the ZEKE spectrum of *para*-difluorobenzene (Figure 3, bottom),[33] which reveals a much clearer vibrational structure than the time-of-flight photoelectron spectrum (Figure 3, top).[34] ZEKE spectroscopy has now also been successfully

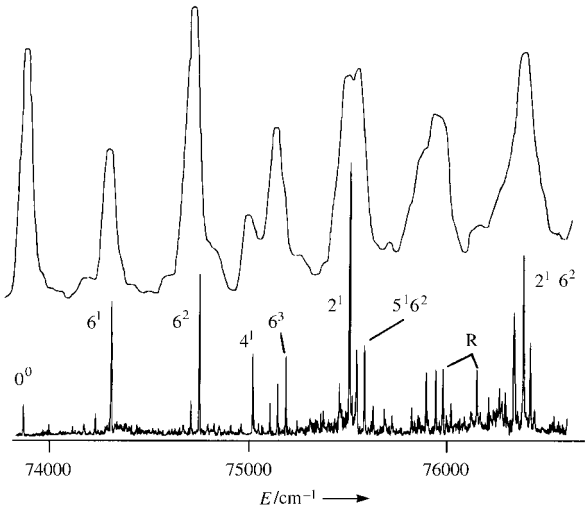

Figure 3. The time-of-flight photoelectron spectrum[34] (top) and ZEKE spectrum[33] (bottom) of *para*-difluorobenzene through the $S_1 6^1$ intermediate state. The improvement in vibrational resolution obtained in ZEKE spectroscopy is illustrated. R = accidental resonances of the second laser in the S_1 state.

applied to studies of the vibrational structure of molecular[35,36] and metal clusters[37–39] and systems with hydrogen bonds.[18,40–46] With ZEKE spectroscopy ionization energies E_i can be determined with an accuracy comparable to that of Rydberg extrapolations but with less experimental effort, even if Rydberg series are not resolved.[25]

2. Experimental Details of the ZEKE Method

The idea and principles of ZEKE spectroscopy have already been discussed in a number of papers,[13,14,23,26,47,48] and other reviews.[15–22,27,51,153] The term ZEKE spectroscopy is now commonly used to describe any experimental technique that detects electrons in a small, experimentally adjustable energy range around (i.e., above and below) a selected ionization threshold with delayed pulsed electric field extraction[13,14] (for a discussion of the older threshold techniques and their relation to ZEKE spectroscopy, see references [15,19]). In contrast to PES, in which a fixed photon energy is used for ionization, the ZEKE method involves the detection of electrons that are formed with zero kinetic energy when the light source is scanned across the region of the ionic threshold. ZEKE electrons (within a certain bandwidth) are produced when the energy of the incident light matches the energy of a rovibronic transition between the initial state of the neutral molecule and the final state of the ion.[15] It should be noted that there are two different ways to produce electrons that contribute to the measured ZEKE signal (Figure 4). First, there are electrons with very low

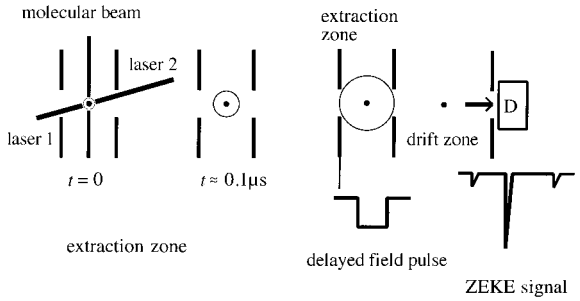

Figure 4. Principle of delayed pulsed field extraction. ZEKE electrons remain at their original position (assuming field-free conditions), whereas kinetic electrons disperse with increasing delay time. The delayed field pulse extracts the ZEKE electrons, which are measured by the detector (D).

kinetic energy, which are generated by photoionization at the threshold (a threshold implies, for molecules, a rovibronic eigenstate of the cation). These "free ZEKE electrons" are discriminated from kinetic electrons with the steradiancy principle[5,15,49] and time-of-flight separation.[50] Secondly, as discovered by Reiser et al.,[28] electrons from long-lived Rydberg levels of high principal quantum number n very close to the threshold contribute significantly to the ZEKE signal or even constitute the observed ZEKE signal (Figure 5). Such electrons are generated by pulsed-field ionization of these high-lying ZEKE Rydberg states from the magic region (see below). The free ZEKE electrons, however, can

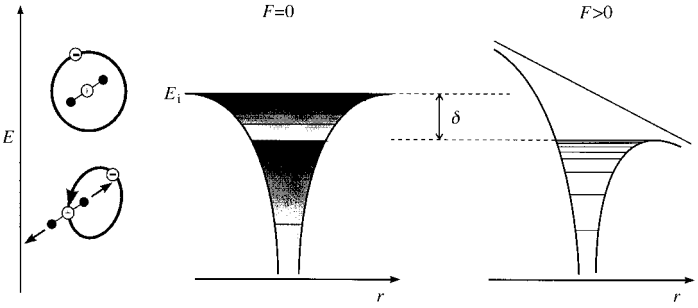

Figure 5. Schematic representation of the magic region of long-lived ZEKE Rydberg states (left) and pulsed-field ionization (right).

contribute to most of the signal when the bandwidth of the ionizing radiation is comparable or larger than the magic region of the long-lived ZEKE Rydberg states. This is typically the case for ZEKE experiments with VUV synchrotron radiation employing a normal incidence monochromator.[50]

The experimental observation of long-lived (up to tens of microseconds) Rydberg states which converge to rovibronic energy levels of the ion has led to the currently most commonly used ZEKE technique, the detection of pulsed field ionized Rydberg electrons.[28] Long-lived Rydberg states with a high quantum number n are clearly evident even in large molecules such as benzene[32] and molecular clusters[18,40–46,51] as well as in small molecules such as NO. These ZEKE Rydberg states which can be ionized by a pulsed field (by diabatic ionization that is described by $E \approx 4\sqrt{F}$, where E is the energy in wavenumbers and F the field strength in $V\,cm^{-1}$)[24] as depicted in Figure 5 owe their longevity to the fact that the electron no longer interacts with the core. For Rydberg states with a low quantum number n (Figure 6) the

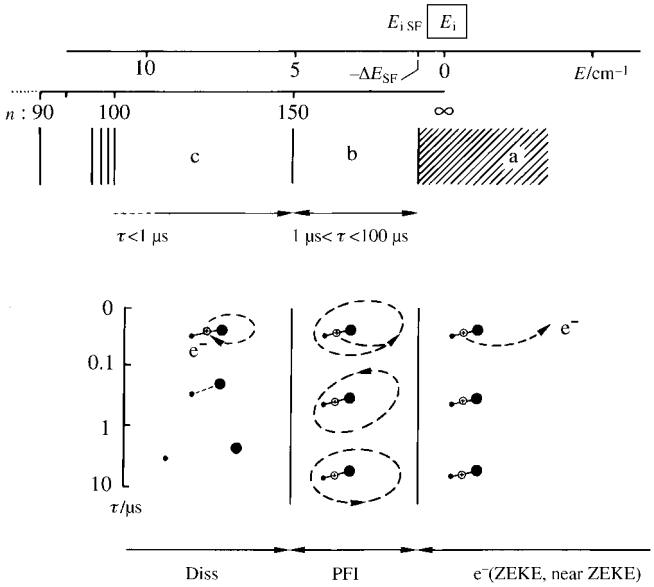

Figure 6. Stabilization of ZEKE Rydberg states in the magic region (b), a few wavenumbers below the ionization threshold (a). The Rydberg states below the magic region (c) predissociate into neutral fragments since the Rydberg electron still collides with the ion core. In the magic region the electron no longer collides with the core, and intramolecular relaxation processes are hence quenched. Diss = dissociation, PFI = pulsed-field ionization, SF = stray field, E_{iSF} = ionization energy in the strong field of the apparatus, τ = lifetime.

Rydberg electron still collides with the core, leading to intramolecular relaxation and particularly to predissociation into neutral products. This accounts for the surprising observation that bandwidths in ZEKE spectroscopy are generally not larger than 5 to 10 cm^{-1}, even when the height of the field pulse is increased, since the lower Rydberg states that would be ionized by the higher field pulse will decay in the field-free delay period (typically several microseconds). From an experimental point of view, this makes it particulary easy to obtain a ZEKE signal if a resolution a few wavenumbers is acceptable.

ZEKE-PFI can be used in combination with a slowly rising electric field extraction pulse (i.e., with a linear or multistep slope)[17,20,25] to obtain the very high resolution (up to 0.2 cm^{-1}) which is essential for the rotational resolution of larger molecules such as benzene.[32,52,53] By a variation of the pulse slope, the spectral resolution of the ZEKE-PFI technique can be adjusted in accordance with the laser bandwidth and the needs of the system under study, that is, whether vibrational or rotational resolution is necessary. This is demonstrated in Figure 7, in which the effect of the slope

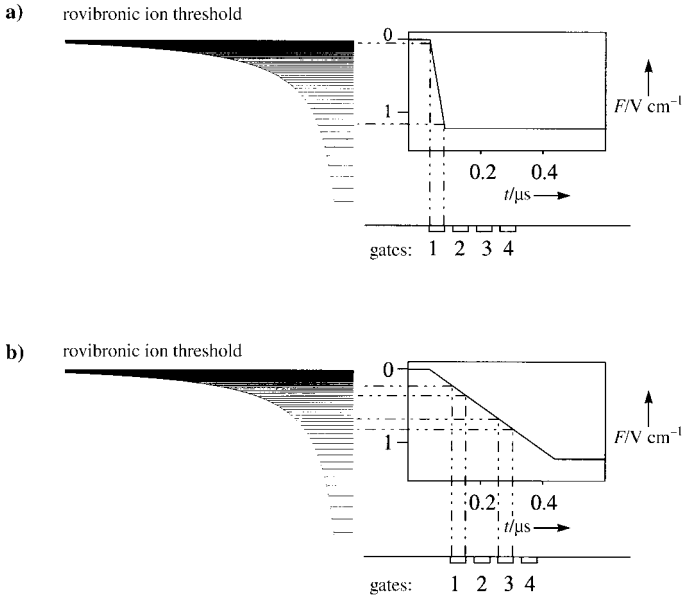

Figure 7. PFI of long-lived ZEKE Rydberg states with a) a fast-rising and b) a slow-rising pulse and detection within a certain time gate.

risetime of the pulse on the time-of-flight of the corresponding electrons produced by PFI is shown. A fast pulse generates the whole signal within a narrow time-of-flight distribution (Figure 7a), whereas a slow pulse spreads the different "slices" of Rydberg states into a broader time-of-flight distribution. By setting a time-of-flight gate and scanning the photon energy of the light source, a smaller spectral "Rydberg slice" is collected for a slow pulse than for a fast pulse. In fact, using a multistep staircaselike extraction pulse provides a method for the exact determination of the ionization energy under field-free conditions.[25,54] Recently, a new technique which employs an inversion of the orientation of two field pulses to selectively ionize "red" or "blue" Stark states was used to gain a further improvement in spectral resolution.[23] An initial (offset) electric pulse selectively ionizes the more easily ionizable red Stark states (lower in energy), while the blue states (higher in energy) survive until a second (probe) pulse is applied in the opposite direction, shifting the blue states to lower energies. The offset:probe ratio can be tuned to produce optimum ZEKE resolution.

The origin of the long lifetime of the ZEKE Rydberg states is still under heavy discussion, and different models have been invoked. Theoretical approaches to these questions can provide new insight into the dynamics of molecular ZEKE Rydberg states.[55–58] Small fields leading to "l mixing" seem to be involved, maybe with some intramolecular coupling.[59–61] The role of ions in the probe volume,[62,63] giving rise to inhomogeneous fields, is not yet fully understood since ion densities can vary over many orders of magnitudes in different experiments. Nonetheless, these theoretical concerns are not ultimately important for the experimental chemist, and the overall message that should be stressed is that long-lived Rydberg states exist in the magic region for all neutral systems, the region in which the ion core and the electron no longer interact.

It should be noted that the PFI technique is not applicable to photodetachment studies of anions, because no Rydberg states exist for these species. The original ZEKE method[13,14] involving the detection of free electrons with negligible kinetic energy must be applied, but it can still yield the vibronic structure of the corresponding neutral molecule.[38,64–66] The ZEKE photodetachment spectrum of IHI^- (Figure 8) is particularly interesting, as it provides an example

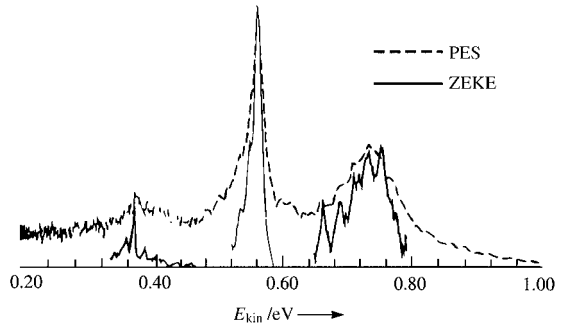

Figure 8. Comparison of the ZEKE spectrum[65] (solid line) and photoelectron spectrum (dashed line) of IHI^-[66] (ν_3 vibration of the [IHI] transition state.

of transition state spectroscopy. The spectrum displays resolved vibrational structure of the (metastable) activated complex $[IHI]^{\neq}$ of the reaction of iodine with hydrogen.[65] This structure was not resolved by PES, as illustrated by the superimposed photoelectron spectrum[66] in Figure 8.

A schematic representation of the experimental setup for a ZEKE experiment is shown in Figure 9. The apparatus consists of a laser system and a vacuum apparatus that contains a molecular-beam source, extraction plates, and a μ-metal shielded flight tube with an electron detector (i.e., dual multichannel plates) at its end. In a typical two-color experiment both dye lasers (typically frequency doubled) are pumped simultaneously by an excimer laser or a Nd:YAG

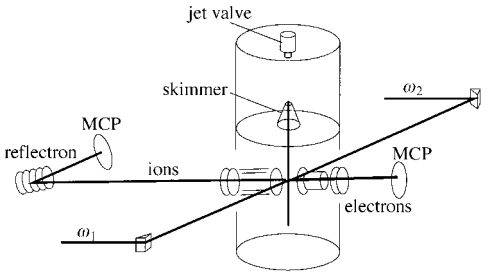

Figure 9. Schematic representaion of a ZEKE apparatus for a two-color ZEKE experiment. MCP = multichannel plate (the detector), ω_1 = frequency of the pump laser, ω_2 = frequency of the ionization laser.

laser. The first dye laser excites a specific vibronic or rovibronic level of an intermediate state, and the second dye laser ionizes the molecules or promotes them into long-lived Rydberg states ($n > 150$), which converge to (ro)vibronic levels of the electronic ground state or an electronically excited state of the cation. After a delay time of several microseconds, an extraction pulse is applied by either a simple electric pulsing device or an arbitrary function generator. The electrons are detected with multichannel plates, and their time-of-flight signal is recorded with boxcar integrators or a transient digitizer by setting narrow time gates (10–30 ns).

3. ZEKE Spectra of Small Molecules

3.1. Nitric Oxide

Nitric oxide was chosen in 1984 for the first ZEKE study with the C $^2\Pi$ as intermediate since it was expected to display a clear rotational structure owing to its low moment of inertia. In a subsequent investigation the A $^2\Sigma^+$ state was selected as the intermediate resonance state[67] and different transitions were used to populate certain rotational levels in the A state. This A state is a 3*s* Rydberg state with a contribution of 94% s, 5% d, and 0.2% p orbitals.[68] As it shows very small spin–rotation splitting, the state is well described by Hund's coupling case b (the standard case when the electron spin is not coupled to the molecular axis).[48,67]

The ZEKE spectra for photoionization through the rotation states $N_A = 0$ to 2 (total angular momentum quantum numbers excluding electronic spin) for the A state are presented in Figure 10. A decrease in intensity for ionizing transitions that involve a change in rotational quantum number (i.e., $\Delta N^+ = N^+ - N_A \neq 0$) is observed as the rotational quantum number N_A increases.[69] This effect is well understood from the theoretical work of Rudolph et al.[68] in which the matrix elements for the continuum partial wave channels were obtained by an ab initio calculation. The second observation is the dependence of the nondiagonal ionizing transitions on the initial rotational quantum number N_A. For example, for $N_A = 2$ one observes a very strong increase in intensity for rotational transitions with $N^+ = -1$ and -3. This effect—that is, the higher intensity of transitions involving a negative N^+ compared to a positive N^+—is observed in other rotationally resolved ZEKE measurements[19,22,70–74] and has been attributed to coupling between the ZEKE Rydberg states high n and those with low n.[71]

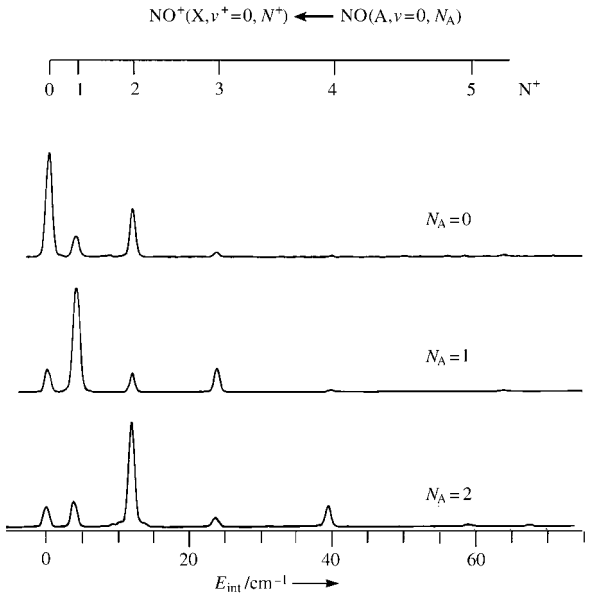

Figure 10. Rotationally resolved ZEKE spectra of NO through different rotational levels ($N_A = 0-2$) of the A $^2\Sigma^+$ ($v = 0$, N_A) state.[69] The spectra illustrate the ionization into different rotational states of the NO^+ cation.

3.2. Iodine

An interesting new class of experiments have probed the dynamics of ZEKE electron, for example spin-orbit autoionization. The ZEKE spectrum of I_2 was extensively studied through different intermediate Rydberg states by Cockett et al.[72–74] A (2+1) REMPI process was used to select the intermediate state, while the energy of the third photon was tuned to obtain the ZEKE spectra. The $[^2\Pi_{3/2}]_{core}5d;2_g$ Rydberg state at around 62600 cm^{-1} was used as intermediate state for ionization into the lower ionic spin-orbit state, and the $[^2\Pi_{1/2}]_{core}5d;2_g$ Rydberg state at around 68000 cm^{-1} for ionization into the upper spin-orbit state. In the original work these states are referred to as 7*s* states.[72,73] However, the assignments given do not conform to a recent reassignment of all ns Rydberg states of I_2 and Br_2 with $n > 6$ to $(n-2)$d Rydberg states following a band-contour analysis of the REMPI spectra of Br_2.[75] One goal of the study was to resolve the question of whether the spin-orbit branching ratios in the ZEKE experiment reflected those observed in a conventional photoelectron spectrum. Spin-orbit autoionization processes can influence the distribution of peak intensities in the ZEKE spectrum, leading to a reduction of spectral intensity in the upper spin-orbit band which is offset by increased intensity in the lower spin-obit state.

The two-color (2+1′) ZEKE spectra of I_2 ionized by the band origin of the $[^2\Pi_{3/2}]_{core}5d;2_g$ Rydberg state at 62639 cm^{-1} as well as by the first three vibrationally excited levels are presented in Figure 11. For the excitation of the band origin (Figure 11 a) the most intense peak corresponds to the $\Delta v = 0$ transition to the $v^+ = 0$ state of the ion. The total energy for the transition to this level is 75069 ± 2 cm^{-1} and represents the adiabatic ionization energy to the ion ground state. A weak vibrational progression built upon the origin band extends up

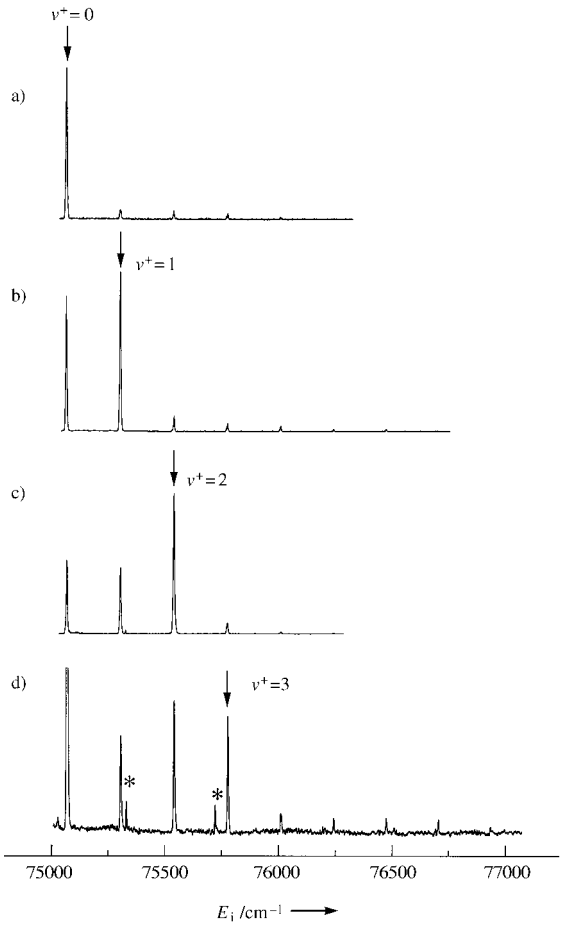

Figure 11. (2+1′) ZEKE spectrum of I_2 recorded through the $[^2\Pi_{3/2}]_{core}5d;2_g$ Rydberg excited state.[72] The vertical arrows indicate the $\Delta v=0$ transitions, and the asterisks accidental $A \leftarrow X$ neutral resonances.

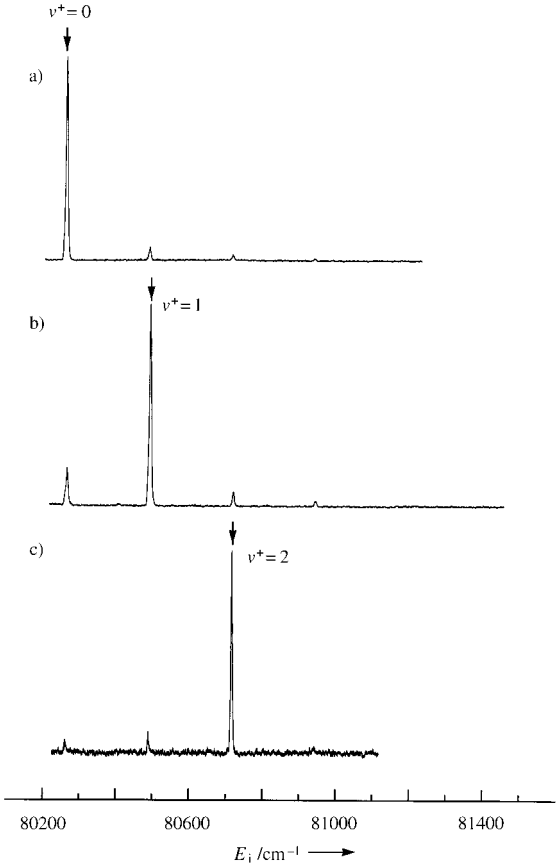

Figure 12. (2+1′) ZEKE spectrum of I_2 recorded through the $[^2\Pi_{1/2}]_{core}5d;2$ Rydberg excited state.[72] The vertical arrows indicate the $\Delta v=0$ transitions.

to $v^+=4$. The minimal geometry change experienced by the molecule upon ionization is reflected in the dominance of the origin peak; this is exactly what one expects for ionization from a Rydberg state. However, the progression does extend to higher v^+ values than one would expect merely on the basis of Franck–Condon factors. For the $v^+=1$ intermediate state (Figure 11b) this behavior is even more pronounced. Again the $\Delta v=0$ transition dominates, but the $v^+=0$ peak appears with nearly the same intensity as the $v^+=1$ peak. The stretching progression can be followed up to $v^+=7$. For intermediate states $v^+=2$ (Figure 11c) and $v^+=3$ (Figure 11d), this behavior becomes more and more pronounced. Although there is an emphasis of the $\Delta v=0$ transition in all the spectra, the distribution of peak intensities cannot be described by a Franck–Condon envelope.

A rather different vibrational pattern was found in the upper spin-orbit state. The two-color (2+1′) ZEKE spectra of I_2 ionized through the band origin of the $[^2\Pi_{1/2}]_{core}5d;2_g$ Rydberg state at 67992 cm^{-1} as well as through the first two vibrational levels are presented in Figure 12a–c. In the spectrum recorded through the band origin (Figure 12a) the most intense peak corresponds to the $\Delta v=0$ transition to the $v^+=0$ level of the ion. The corrected total transition energy to the origin is 80266 ± 2 cm^{-1}, which corresponds to the adiabatic ionization energy into the upper $^2\Pi_{1/2}$ spin-orbit state. This result, combined with the ionization energy for the lower $^2\Pi_{3/2}$ spin-orbit state, gives rise to an improved spin-orbit splitting constant for I_2^+ in its ground electronic state of 5197 ± 4 cm^{-1}. For the upper spin-orbit component, increasing the level of vibrational excitation in the intermediate Rydberg states leads to a marked propensity for the $\Delta v=0$ transition. This corresponds to classic Franck–Condon behavior.

The intensities in the lower spin-orbit state spectrum that do not correspond to Franck–Condon behavior were interpreted in terms of an autoionization mechanism involving a Rydberg series which converges to a higher ionic vibrational state. The ZEKE states with low n converging to higher thresholds interact with nearly degenerate ZEKE Rydberg states with high n in this region and can be ionized by the pulsed electronic field applied in ZEKE-PFI. There are no comparable states located in the vicinity of the upper spin-orbit state to perturb the intensities.

In an extension of this study, ionization of I_2 was studied through the valence B state. Owing to the valence character of the intermediate state, the ZEKE spectra into both spin-orbit components of the cation exhibit very long Franck–Condon progressions. For the lower spin-orbit component, an extended vibrational progression up to at least $v=62$ is found, while the progression in the upper state can be followed as far as

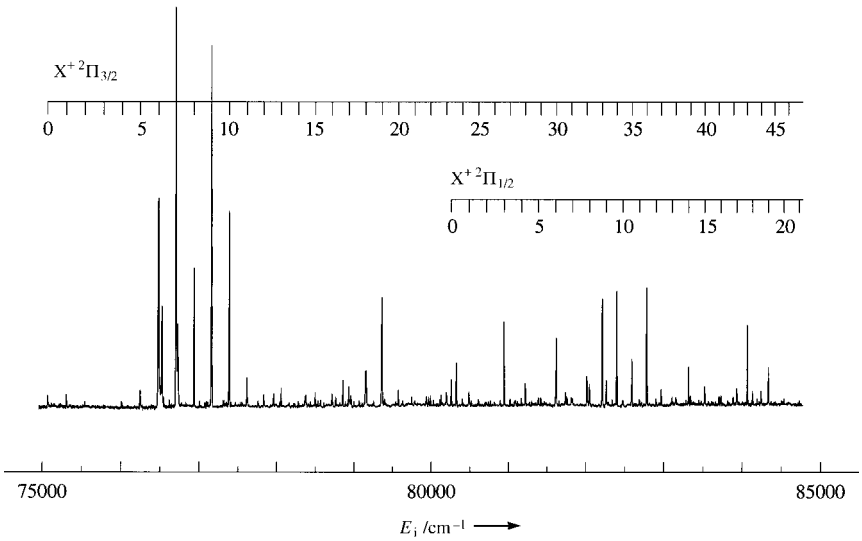

Figure 13. (1+2′) ZEKE spectrum of I_2 recorded through $v = 15$ of the valence $B\,^3\Pi_u 0_u^+$ excited state with a long Franck – Condon-forbidden progression in the $X^+\,^2\Pi_{3/2}$ state of the iodine cation.[72]

$v = 34$. The (1+2′) ZEKE spectrum of I_2 in the energy range 75000 to 85000 cm^{-1} recorded through $v = 15$ of the valence B state[73] is shown in Figure 13. Although the extent of the vibrational progressions can be adequately simulated through the calculation of Franck – Condon factors, the distribution of peak intensities and observed orbit branching ratio reflects the considerable contribution of both spin-orbit and field-induced resonant autoionization processes. In addition, accidental resonances at the two-photon level with ion-pair states further perturb the distribution of peak intensities.

3.3. Hydrogen Bromide

ZEKE spectroscopy has been used to follow the dynamics of photodissociation[76] and predissociation in a variety of small molecules.[77–81] Hepburn et al.[82] recently recorded ZEKE spectra for the $v^+ = 1-3$ levels of the predissociating $A\,^2\Sigma^+$ state of HBr^+ by VUV excitation of high Rydberg states of HBr converging to the predissociating level. The ZEKE-PFI spectra were obtained with rotational resolution for both predissociating ($v^+ = 2,3$) and nondissociative levels. For the dissociating levels, field ionization occurs long after the ion core has fragmented; the Rydberg electron is unperturbed by the dissociation. Therefore, the spectrum results from field ionization of a Br atom in a high Rydberg state, which is produced by predissociation of the initially excited HBr Rydberg state. The intensities and lineshapes of the nondissociating $v^+ = 1$ level and the predissociating $v^+ = 2$ level were comparable, demonstrating that the initially excited Rydberg electron is essentially undisturbed by the dissociating core. The $v^+ = 3$ level was considerably broadened, however, consistent with a lifetime of only 10^{-13} s. Adiabatic decay of high-lying Rydberg states converging to predissociating levels of the respective ions has also been observed in ZEKE-PFI of van der Waals complexes (see Section 8.1).

3.4. Ammonia

Ammonia, NH_3, was the first polyatomic molecule studied by ZEKE spectroscopy[47] for which the full rotational resolution in the cation was achieved in 1991. (An earlier study of benzene by Chewter et al.[83] showed a partially resolved rotational structure which was not fully assigned.) Ionization was achieved by (2+1′) one-color REMPI excitation with the $\tilde{B}$ state as intermediate resonance excited through the two-photon transition $\tilde{B} \leftarrow \tilde{X}$. The excitation spectrum for the 2_0^2 transition obtained by a (2+1′) REMPI ion signal measurement shows clearly resolved rotational structure with Coriolis interaction and *l*-type doubling, allowing for rotational-state selectivity in the intermediate state. Two rotational states corresponding to the *ortho* and *para* nuclear-spin modifications of NH_3, that is, J',K':3,1 (*ortho*-NH_3) and J',K':3,2 (*para*-NH_3), were chosen as intermediate states for the ZEKE spectra.

The ZEKE spectra obtained from the two selected rovibronic levels of the $2^2\tilde{B}$ state (Figure 14), measured in the energy range between 21800 and 22300 cm^{-1} for the ionizing (probe) laser, correspond to the $v_2^+ = 1$ vibrational quantum number of the ion. There is a striking difference between the spectra obtained for *ortho*- (top spectrum) and

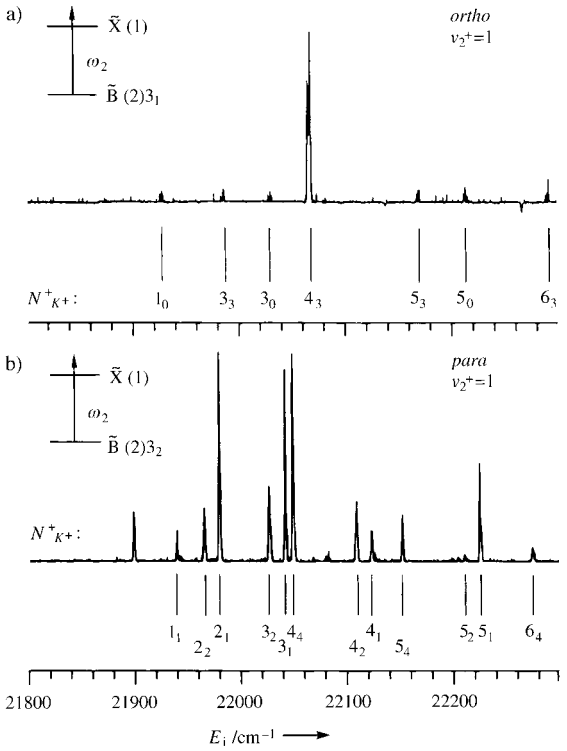

Figure 14. Rotationally resolved ZEKE spectra of the $v^+ = 1$ band of NH_3 through the $\tilde{B}(v = 2)$ state with a) $J = 3$, $K = 1$ (*ortho*-NH_3) and b) $J = 3$, $K = 2$ (*para*-NH_3).[47]

para-NH_3 (bottom spectrum). The ZEKE spectrum of *ortho*-NH_3 shows only a single transition into the ion rotational state with N^+,K^+:4,3; there are additional transitions into $K^+=0$ and 3 which are weaker by at least an order of magnitude. On first sight this ZEKE spectrum looks as if it originates from the photoionization of an atom. In contrast, the ZEKE spectrum of *para*-NH_3 shows many more transitions with the strongest for $K^+=1$ and $N^+=4$, $K^+=4$ and some weaker transitions into $K^+=2$. The symmetry selection rules that apply to ZEKE transitions can account for the main spectral features.[48]

3.5. The Renner–Teller Effect in the *trans*-Bending Vibration of the Acetylene Cation.

Linear molecules such as acetylene in degenerate electronic states (e.g. the ground state $\tilde{X}^+{}^2\Pi_u$ of $C_2H_2^+$[84] exhibit a form of vibronic coupling that is termed the Renner–Teller effect.[1] The acetylene cation is of particular interest because it shows a Renner–Teller interaction that is expected to dominate both the rotational structure and the spin-orbit splitting. Briefly, the vibrational angular momentum l generated by the bending mode leads to a vibronic angular momentum $K=|\lambda+l|$, where λ is the projection of the electronic orbital angular momentum along the internuclear axis. For the $\tilde{X}^+{}^2\Pi_u$ state of the acetylene ion, the spin is coupled to λ giving ω, which is then coupled to l to give $P=\omega+l$, the vibronic angular momentum including spin. A schematic energy diagram for the Renner–Teller levels of the v_4^+ *trans*-bending operation of the $\tilde{X}^+{}^2\Pi_u$ state of the acetylene cation is shown in Figure 15. In the ZEKE experi-

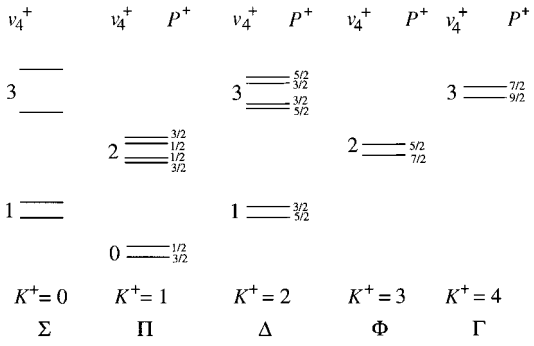

Figure 15. A schematic energy level diagram for the Renner–Teller levels of the v_4^+ *trans*-bending vibration of the $\tilde{X}^+{}^2\Pi_u$ state of the acetylene cation.[85]

ments carried out by Pratt et al.[85] it was not only possible to resolve the Renner–Teller splitting but also the spin-orbit and rotational structure of the $^2\Pi_u$ state of the cation. The full level structure of this system and the selection rules, including the parity selection rule, are discussed in reference [85]. The additional vibronic bands that appear in these spectra can be explained by relaxation of symmetry selection rules that arises through the Renner–Teller effect. Figure 16 gives an overview of the ZEKE spectrum in the region between the $^2\Sigma_u^+$ and the $^2\Sigma_u^-$ components of the $v_4^+=1$ vibronic band, which are obtained by pumping the $R(1)V_4^0K_0^1\tilde{A}^1A_u\leftarrow\tilde{X}^1\Sigma_g^+$ transition of neutral acetylene.[86,87]

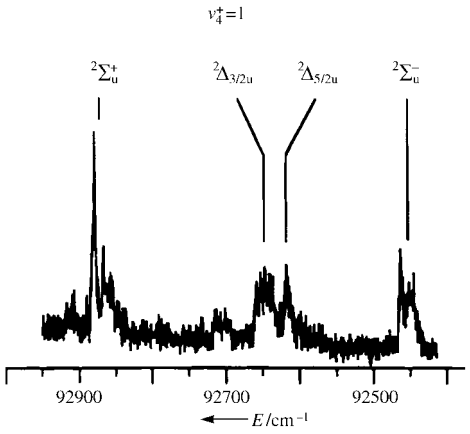

Figure 16. ZEKE spectrum of acetylene in the region of $v_4^+=1$ through the $R(1)V_4^0K_0^1\tilde{A}^1A_u\leftarrow\tilde{X}^1\Sigma_g^+$ transition in the neutral molecule.[86,87]

3.6. Carbon Dioxide

The carbon dioxide cation with its $\tilde{X}^+{}^2\Pi_g$ ground state is also subject to a Renner–Teller interaction. A thorough ZEKE study of this molecule with use of VUV single-photon ionization was carried out by Softley et al.[88] They resolved the different Renner–Teller states ($^2\Pi_{g3/2}$, $^2\Pi_{g1/2}$, $^2\Delta_{u5/2}$, $^2\Delta_{u3/2}$, $^2\Sigma_u^+$, and $^2\Sigma_u^-$) and found that the propensity rules for angular momentum transfer during photoionization are very strongly dependent on the vibronic symmetry of the different ionic states. This has to do with the different Hund's coupling cases that apply to each of the different vibronic cation states. The spectral region studied in these experiments comprises the transitions from the ground vibronic state of CO_2 [$\tilde{X}^1\Sigma_g^+(000)$] to the two spin-orbit components of the ground state of CO_2^+ [$\tilde{X}^+{}^2\Pi_{g3/2}/\tilde{X}^+{}^2\Pi_{g1/2}$ (000)] as well as to the four Renner–Teller

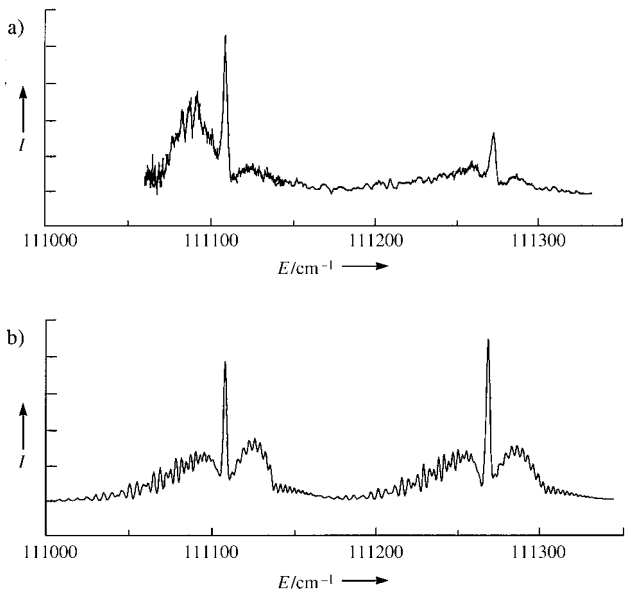

Figure 17. a) Experimental[88] and b) simulated[89] one-photon ZEKE spectrum of CO_2 corresponding to the $\tilde{X}^+{}^2\Pi_{g,i}(000)$ $(i=1/2,\ 3/2)\leftarrow\tilde{X}^1\Sigma_g^+(000)$ transition.

ionic substates which arise when one quantum of the bending vibration is excited ($\tilde{X}^+(010)$ $\mu\,^2\Sigma_u^+$, $^2\Delta_{u5/2}$, $^2\Delta_{u3/2}$, $\kappa\,^2\Sigma_u^-$). The ZEKE spectrum of the $\tilde{X}^{+2}\Pi_{g3/2}/\tilde{X}^{+2}\Pi_{g1/2}$ $(000) \leftarrow \tilde{X}\,^1\Sigma_g^+$ transition is reproduced in Figure 17a. The comparison to the theoretical fit (Figure 17b) using the approach of Buckingham et al.[89] shows that some channel couplings between the ZEKE Rydberg states with high n and those with low n (converging to higher ionization limits) leads to some deviations in intensity and the enhancement of higher angular momentum transfer transitions. The study also revealed a disagreement with a Rydberg extrapolation to the ionization energy of Cossart-Magos et al.[90] The disagreement of 10 cm^{-1} is far too large to be explained as experimental error. It may be that a perturbation in the Rydberg series used for extrapolating to $n \rightarrow \infty$ has not yet been properly accounted for.

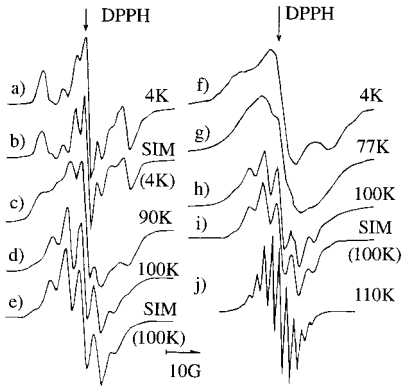

Figure 19. ESR spectra of the benzene cation in freon matrices at temperatures from 4 to 110 K.[100] Spectra (a) – (e) were recorded in $CFCl_3$, while spectra (f) – (j) were obtained in $CFCl_2CF_2Cl$ at various solute concentrations. SIM = simulated spectrum (at the temperature of the previous spectrum), DPPH = diphenylpicrylhydrazyl (standard). At higher temperatures the spectra support a structure of highest symmetry (D_{6h}), whereas at 4 K two different spin densities with intensity ratio 4:2 are found, which supports a distorted D_{2h} structure.

4. ZEKE Spectra of Larger Molecules

4.1. Benzene

The neutral benzene molecule has a hexagonal, planar structure with D_{6h} symmetry.[91–94] In the electronic ground state the electron configuration is $(a_{2u})^2(e_{1g})^4$. Upon ionization, one e_{1g} electron is removed from the highest molecular orbital, thus leaving one e_{1g} electron unpaired. This results in a doubly degenerate $^2E_{1g}$ electronic ground state of the cation. According to the Jahn – Teller theorem,[95] for any nonlinear polyatomic molecule in a degenerate electronic state there exists a distortion of the nuclei along at least one nontotally symmetric normal coordinate. This results in a splitting of the potential energy function, so that the potential minimum is no longer at the symmetrical position.[1,95–97] Several authors have discussed structural distortions of the benzene cation;[98,99] model calculations predict three equivalent D_{2h} structures.[98] These structures could be envisaged as locally distorted (elongated or compressed) structures as shown in Figure 18.

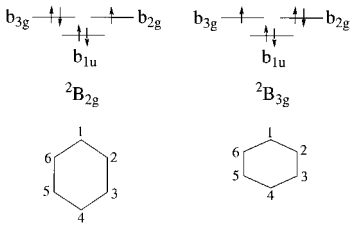

Figure 18. Distorted structures of the benzene cation resulting from removal of an e_{1g} electron from benzene, which corresponds to a reduction in the symmetry from D_{6h} to D_{2h}. The distortion can produce either an elongated (left) or compressed structure (right).

The distortion to D_{2h} symmetry can, in fact, be detected experimentally in a matrix at low temperatures.[100] The ESR spectra of $C_6H_6^+$ in a freon matrix indicate an increased spin density at atoms C_1 and C_4 at 4.2 K but an equivalent spin density at 100 K (Figure 19). Thus, the question arises whether the D_{2h} structure is static and destabilized at higher temperatures by collisions with the matrix or whether a dynamic D_{2h} structure is stabilized by the matrix lattice.

The experimentally determined value of 266 cm^{-1} for the stabilization energy[101] is about the half of the zero-point energy of the lowest Jahn – Teller-active normal vibration. For weak Jahn – Teller coupling the stabilization energy for the distorted symmetry is smaller than the zero-point energy of the Jahn – Teller-active mode. Under collision-free conditions, the three equivalent D_{2h} structures of the cation would dynamically interconvert, and the ground state of the cation would still be described in the D_{6h} symmetry group. For strong Jahn – Teller coupling the cation would spend much time in one of the three structures, and would therefore be described in the D_{2h} symmetry group. The knowledge of the structure and the symmetry of the isolated benzene cation is desirable not only for testing quantum-mechanical model calculations, it is also of fundamental importance for organic chemistry. Rotationally resolved ZEKE spectroscopy allows an unambiguous determination of the symmetry of the cation by analysis of the rotational transitions together with group-theoretical considerations.[1,102]

If one quantum of a Jahn – Teller-active normal vibration (for benzene normal modes with e_{2g} symmetry,[95] ν_{6-9} according to Wilson's notation[103]) is excited, the linear dynamic Jahn – Teller coupling leads to a splitting into two vibronic states with vibronic angular momentum $j = \pm 1/2$ and $j = \pm 3/2$.[1,104] The quadratic dynamic Jahn – Teller coupling further splits the $j = \pm 3/2$ band into two substates, but leaves the $j = \pm 1/2$ state doubly degenerate.[1] The excitation of an e_{2g} normal vibration in an E_{1g} electronic state leads to vibronic states with $B_{1g} \oplus B_{2g} \oplus E_{1g}$ vibronic symmetry. A first-order interaction lifts the fourfold degeneracy and results in two doubly degenerate vibronic states with $B_{1g} \oplus B_{2g}$ and E_{1g} symmetry, respectively. Higher order interactions can split the $B_{1g} \oplus B_{2g}$ state, but not the inherently doubly degenerate E_{1g} vibronic state. An unambiguous assignment of the individual, split vibronic states and an exact determination of their energies is necessary for a precise determination of

the strengths of the vibronic coupling. Rotationally resolved ZEKE spectroscopy is the suitable method for the unambiguous assignment of the symmetry species of the vibronic states and thus the vibrational modes of the benzene cation, thereby providing reliable values for the vibronic coupling strengths.

A first attempt to resolve the question of whether a static or a dynamic D_{2h} structure is applicable was carried out by gas-phase PES.[101] The photoelectron spectrum shown in Figure 20 was obtained with a standard time-of flight technique

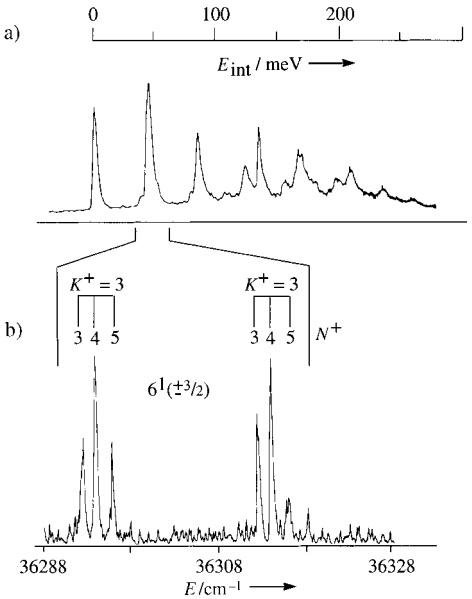

Figure 20. a) Time-of-flight photoelectron spectrum[101] with limited vibrational resolution and b) ZEKE spectrum[32] of benzene showing rotationally resolved $6^1(3/2)$ vibronic bands of the benzene cation.

and two-photon, two-color (1+1′) ionization with the $S_1 6^1$ state as intermediate resonance. The vibrational structure found in that photoelectron spectrum was assigned to the 0^0 vibrational origin and the 6^1 progression; the $6^1(3/2)$ and $6^1(1/2)$ states show linear Jahn–Teller splitting. No resolution of the quadratic Jahn–Teller splitting of the $6^1(3/2)$ state into the B_{1g} and B_{2g} components nor any resolved rotational structure was observed.

The rotational state of an oblate-symmetric rotor is characterized by two quantum numbers (Figure 21). For the ground state S_0 and intermediate states S_1 of neutral benzene, the relevant quantum numbers are J, the total angular momentum, and K, its projection along the principal axis of the molecule. For the benzene cation with electronic spin $S = 1/2$, the rotational states are characterized (assuming a weak spin-orbit interaction) by the quantum number N^+, which describes the total angular momentum without electronic spin, and the projection quantum number K^+. In degenerate vibronic states the rotational states split by Coriolis interactions must be differentiated by an additional quantum number, $\pm l$.[1]

The determination of the rotational structure of the benzene cation and the assignment of the rotational transitions observed in the ZEKE spectra allow the determination of the vibronic symmetry species of the corresponding vibrational state. This is done similarly as for ammonia.[47,48] Starting with the known symmetry species of the intermediate state, in which only one rovibronic state is populated, the possible final states are determined based on group-theoretical considerations. The conservation of symmetry species of the nuclear spin wave function and the selection rules for electronic symmetry species as well as the coupling of angular momenta greatly restrict the possible transitions; depending on the vibronic symmetry species of the final state, only certain rotational progressions can be observed.[32,48]

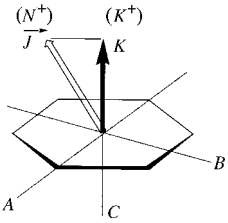

Figure 21. Conventions for benzene as a symmetric rotor. For the neutral molecule the total angular momentum quantum number is denoted J, and its projection onto the highest symmetry axis K; for the cation electron spin is neglected, and total angular momentum is denoted N^+ with projection K^+.

Figure 22 shows the ZEKE spectrum for the transitions into the ion ground state from the intermediate states $S_1 6^1$ ($J' = 1$, $K' = 1, +l$);[32] the rotational states in $S_1 6^1$ are assigned according to reference [93]. The most notable feature in the rotational structure is the appearance of progressions in the

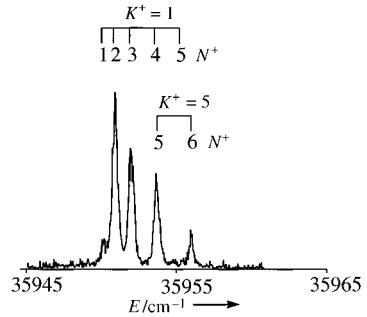

Figure 22. Rotationally resolved ZEKE spectrum of benzene at the vibronic origin (E_{1g}) of the benzene cation through the $S_1 6^1$ ($J' = 1$, $K' = 1$) intermediate state. Two rotational progressions with $K^+ = 1$ and $K^+ = 5$ are observed.[32]

total angular momentum quantum number N^+ (without electron spin) of the cations with $K^+ = 1$ and $K^+ = 5$. For transitions between bound states, the selection rules $\Delta J = 0, \pm 1$ and $\Delta K = 0, \pm 1$ are valid. However, for a transition from a bound to an unbound state, the ZEKE electron can compensate for the angular momentum by vector coupling depending on the type of the partial wavefunction (s, p, d,…), thus enabling higher changes in the rotational angular momentum.[48]

It is interesting to observe the effect of excitation of a Jahn–Teller-active vibrational mode on the structure of the ion and to see how vibronic interactions influence the vibrational structure of the ground state. Because of vibronic coupling, the electronic wave function depends on the vibrational coordinate. According to the Jahn–Teller theorem, excitation of a degenerate vibration in a degenerate electronic state should lift the degeneracy, and splitting into vibronic states of different energies is expected.[99]

For excitation of ν_6, the second component of the ν_6 band with vibronic angular momentum $j=\pm 3/2$ is split due to the quadratic, dynamic Jahn–Teller effect into two states with B_{1g} and B_{2g} symmetry.[104] Since both vibronic states have the same symmetry species B and their rotational constants should be close to each other, very similar rotational structures are expected for the two states. Figure 23 shows the ZEKE

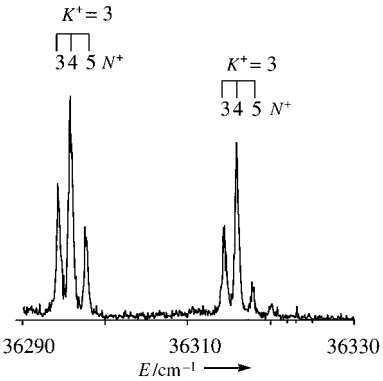

Figure 23. Rotationally resolved ZEKE spectrum of benzene at the lower 6^1 Jahn–Teller manifold $6^1(\pm 3/2)$ through the $S_1 6^1$ ($J'=1$, $K'=1$) intermediate state. The two bands correspond to the B_{1g} and B_{2g} vibronic bands, which are split by the quadratic Jahn–Teller interaction. For each band only one rotational progression with $K^+=3$ is observed.[32]

spectrum through the same intermediate state $S_1 6^1$ ($J'=1$, $K'=1, +l$).[32] Two clearly separated vibronic states with almost identical rotational structures can be seen, which can both be assigned to a progression with $K^+=3$. This leads to the vibronic symmetry species B_{1g} and B_{2g}, in agreement with the symmetry selection rules for ZEKE spectroscopy; these components must be assigned to the two Jahn–Teller states $6^1(j=\pm 3/2)$. The separations of each set of two transitions with the same quantum numbers N^+ and K^+ agree to within ± 0.1 cm^{-1}. The mean splitting between the two states is 20 cm^{-1}.

The differences in the energies of the band origins of the $6^1(j=\pm 1/2)$ bands and the $6^1(j=\pm 3/2)$ bands is 331 and 311 cm^{-1}, respectively. This corresponds to roughly half of the vibrational energy of the ν_6 mode. Thus, the benzene cation is a good example for intermediate coupling, in which the vibrational frequency of the Jahn–Teller-active mode and the accompanying coupling strengths have almost the same values.[32,53,104] With the precise energy values for the components of the ν_6 band that are affected by vibronic interaction, the results of quantum-chemical ab initio calculations can be examined very closely. Comparison with values published in 1992 shows how well these latest dynamic Jahn–Teller calculations can take into account several active modes.[105] The difference between the calculated value for the $6^1(j=\pm 1/2)$ band of 694 cm^{-1} and the measured value of 676.4 cm^{-1} is only three percent.

The determination of the vibronic symmetry species of the vibronic levels of the benzene cation by rotationally resolved ZEKE spectroscopy was recently described for the B_{1g} and B_{2g} bands.[53] The analysis of the ZEKE spectrum for the ν_6 mode led to the assignment of the global minimum of the benzene cation as acute D_{2h}, with the caveat that the energy difference between the distortion isomers on the psuedorotation coordinate is only a few percent of the zero-point energy along this coordinate alone. The cation should therefore be viewed as a fluctional, dynamical D_{6h} structure. The analysis of the full vibrational structure, which is highly irregular due to multiple-mode Jahn–Teller coupling, constitutes a significant contribution to the understanding of the Jahn–Teller effect and vibronic interactions. High-resolution experimental analysis of the cation of benzene, the prototypical aromatic molecule which is frequently the subject of theoretical studies, was not possible previously.

4.2. *para*-Difluorobenzene

The resolution of the vibrational structure of larger molecular ions is also an important application of ZEKE spectroscopy in chemistry. The considerable gain in resolution makes it possible to measure low-frequency vibrations and to analyze combination bands which may be congested in the photoelectron spectrum (see Figure 3). The cation of *para*-difluorobenzene (*p*-DFB), like most large molecular ions, does not fluoresce, making most methods of fluorescence spectroscopy inapplicable. Ab initio calculations from von Niessen et al.[106] predicted an electronic configuration for the outer molecular orbitals of *p*-DFB of $\ldots(b_{2u})^2(b_{3g})^2(b_{3u})^2(b_{1g})^2(b_{2g})^2(a_u)^0(b_{3u})^0$ within the D_{2h} symmetry group. From He^I and He^{II} photoelectron spectra[4,107,108] it follows that the symmetry of the electronic ground state for the *p*-DFB cation is $^2B_{2g}$.

The ZEKE spectrum obtained from excitation through the vibrationless S_1 state is reproduced in Figure 24.[33] The scanning region ranges from the ionization energy to approximately 3000 cm^{-1} higher; the majority of the spectral bands have been definitively assigned to vibrational states of the *p*-DFB cation. Aside from the vertical transition into the vibrationless state of the cation, the spectrum is dominated by transitions into totally symmetric modes and their combina-

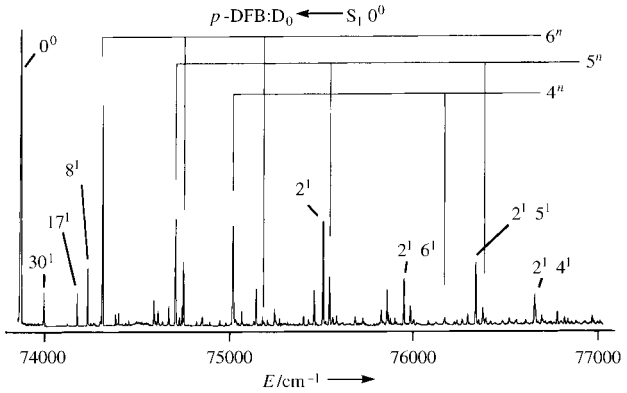

Figure 24. Vibrationally resolved ZEKE spectrum of *para*-difluorobenzene through the S_1 vibrational origin (0^0) as intermediate resonance.[33] D_0: cation ground state.

tion bands. The strongest transitions are the 6^1, 5^1, 4^1, and 2^1 and various combinations of these quanta. However, the modes that are not totally symmetric—ν_{30}, ν_{17}, and ν_8—also appear and occur in combination with a_g modes. Several transitions could not be unambiguously identified in the present analysis.

Figure 25 shows the ZEKE spectrum using $S_1 6^1$ as the resonant intermediate state. For the ν_6 mode, a progression with four quanta is observed with the maximum intensity for the 6^2 level. This shift of the Franck–Condon maximum

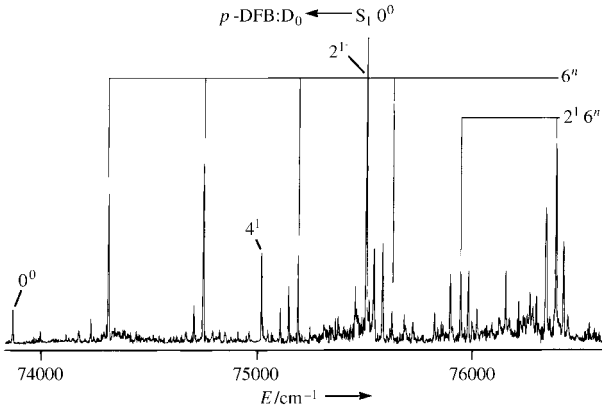

Figure 25. Vibrationally resolved ZEKE spectrum of *para*-difluorobenzene through the $S_1 6^1$ state as intermediate resonance.[33] D_0: cation ground state.

towards higher vibrational excitation in the ν_6 mode was also observed in the corresponding time-of-flight photoelectron spectrum.[34] Again, the ZEKE spectrum mainly displays transitions into symmetric modes. Probable assignments, taking into account the combination bands, have also been given in reference [34]. The most prominent feature of this ZEKE spectrum is the strong activity of the a_g modes $\nu_2-\nu_6$ (the a_g vibration ν_1 has not yet been seen in conventional photoelectron spectra and is, with the exception of the ZEKE spectrum from the $S_1 0^0$ state, outside the scanning range employed in the experiments reported here).

The restricted validity of the $\Delta v = 0$ propensity rule for *p*-DFB should be noted at this point. This propensity has previously been observed for the ionization of aromatic molecules from their S_1 states.[109] The failure of the rule is not so surprising though, as it is only expected to hold when the geometries of the S_1 and ionic states are similar (as they are, for example, for Rydberg states and their corresponding ions). Different vibrational excitations of the S_1 state produce some bands in combination with one quantum of mode ν_6, which are of similar strength as the dominating $\Delta v = 0$ transitions ($D_0 30^1 6^1 \leftarrow S_1 30^1$, $D_0 9^2 6^1 \leftarrow S_1 9^2$, $D_0 17^1 6^1 \leftarrow S_1 17^1$). The Franck–Condon maximum is observed for the 6^2 vibration of the cation for excitation through the $S_1 6^1$ intermediate state, which is in agreement with the previously published photoelectron spectrum[34] (the stronger appearance of the 2^1 band in the ZEKE spectrum pumping the $S_1 0^0$ is due to the dye-tuning curve). The shift of the Franck–Condon maximum towards 6^2 implies that the geometries of the S_1 state and the ionic state differ along this mode, so that maximum overlap is achieved for the first overtone in the ion rather than the fundamental.

Within the Franck–Condon approximation (and in the absence of any other coupling) no transitions should be observed for which the symmetry species of the vibrational wavefunction in the S_1 state is different from that of the ion. The most prominent transitions which violate this symmetry restriction are the ν_8, ν_{17}, and ν_{30} vibrations. Vibronic coupling (to an excited electronic state) in the cation cannot explain the occurrence of these three vibrations of different symmetry, and the origin of such symmetry-forbidden vibrations is still not perfectly clear. A possible mechanism could be channel couplings between Rydberg states with high n and those with low n converging to higher limits.

To aid in the assignment of the observed vibrations in the *p*-DFB cation and to check the experimentally observed vibrational frequencies, ab initio calculations were performed.[33] The calculations support the experimental assignments for the ionic frequencies and lead to a D_{2h} structure for the S_0 and the ionic ground state. For the S_1 state deviations from the D_{2h} symmetry, mainly along the ν_8 coordinate, are indicated.

4.3. Pyrazine

Pyrazine has long served as a model for understanding intersystem crossing, since the S_1-T_1 gap is small enough that there are a limited number of zero-order triplet states isoenergetic to a given singlet level. The spin-orbit interaction of T_1 and S_1 produces a set of mixed singlet–triplet states (molecular eigenstates). Hillenbrand et al.[110] used ZEKE spectroscopy to study the degree of singlet–triplet mixing. The ZEKE spectrum they measured as function of energy above the first ionization limit for an excitation wavelength of the first laser corresponding to the $S_1-S_0 0-0$ transition is reproduced in Figure 26. Surprisingly, they observed not only the expected transitions from S_1 to the electronic ground state of the ion (Figure 26, left) but also transitions from T_1 (Figure 26, right). The population of the triplet state T_1, under the experimental conditions, is mediated through

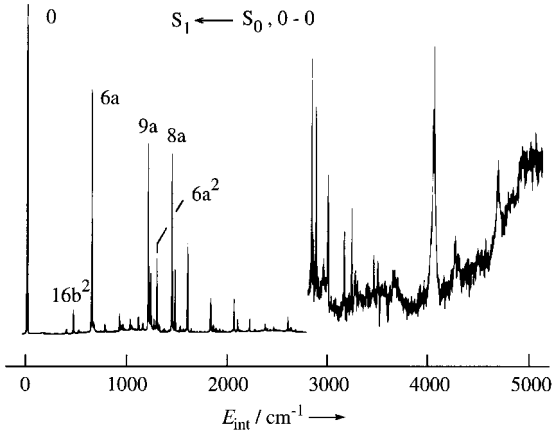

Figure 26. Vibrationally resolved ZEKE spectrum of pyrazine through the $S_1 0^0$ intermediate state.[110]

pyrazine – argon clusters. The intersystem crossing is enhanced in the cluster, and evaporation of argon molecules produce a cold triplet monomer. With the assignment of the vibrations in the pyrazine ion, the lines associated with ionization of the triplet states were also assigned (including some vibrational structure of the triplet state itself).

5. Torsional Motions Observed in ZEKE Spectroscopy

5.1. Internal Rotation in the Toluene Cation

The occurence of motion of large amplitudes, for instance in molecular clusters (see below) or in systems with internal rotors (e.g. methyl groups), has been followed with considerable interest in the last few years. The ZEKE spectroscopic measurements of toluene by Weisshaar et al. offer the opportunity to study how such systems behave upon ionization.[111] The description of the toluene molecule and its torsional states relies on its rigorous classification according to its irreducible representations in the molecular symmetry group G_{12},[102] which is isomorphic to the point group D_{3h}.

The problem of an unhindered, rigid methyl rotor attached to a rigid frame is reduced to a one-dimensional Schrödinger equation. The eigenfunctions are $\Phi_{tor}(\alpha) = (2\pi)^{-1/2} e^{\pm im\alpha}$ with the eigenvalues $E_m = Bm^2$, where B is an effective constant for the rotation of the methyl group relative to the rigid molecular framework and $m = 0, \pm 1, \pm 2, \ldots$ is the rotational quantum number. In toluene the torsional potential has sixfold symmetry. A small torsional perturbation of the form $V(\alpha) = (V_6/2)(1 - \cos 6\alpha)$ leaves the $m = \pm 1$, ± 2, ± 4, and ± 5 states doubly degenerate but lifts the degeneracy of the $m = \pm 3$ and $m = \pm 6$ levels. One defines $\alpha = 0$ when one C–H bond is in the plane of the benzene ring (eclipsed geometry); when $\alpha = \pi/6$, one C–H bond is perpendicular to the ring (staggered geometry). In order of increasing energy (Figure 27), the rotor states are $0a_1'$, $1e''$, $2e'$, $3a_2''$ and $3a_1''$ (or vice versa), $4e'$, etc. Band intensities in the $S_1 - S_0$ and cation – S_1 spectra reveal which $|m| = 3$ state lies lower in energy and thus the absolute phase of the torsional potential. For negative V_6 (potential minimum at $\alpha = \pi/6$) $3a_2''$ lies below $3a_1''$, whereas for positive V_6 (potential minimum at $\alpha = 0$) $3a_1''$ lies below $3a_2''$, as in the ground state of toluene.

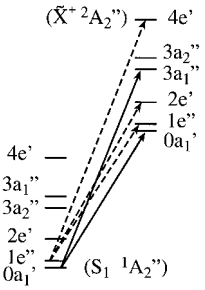

Figure 27. Nearly free rotor states and G_{12}-symmetry species for toluene (S_1) and the toluene cation. The arrows indicate the strongest ZEKE transitions (for $\omega_1 = 37475\ cm^{-1}$), which correspond to the 0 – 0 and 1 – 1 rotor transitions of $S_1 \leftarrow S_0$. Note the different order of the $3a_1''$ und $3a_2''$ levels in S_1 state and the cation.[111]

In the absence of coupling between torsion and molecular rotation or between torsion and electronic motion, allowed transitions must preserve torsional-state symmetry: $\Gamma_{tor}' \otimes \Gamma_{tor}'' \supset a_1'$. Accordingly, the $0a_1'$ and $1e''$ states of S_0 populated in the beam allow transitions only to a_1' and e'' states of S_1. However, next to the overlapping $0-0(a_1' \leftarrow a_1')$ and $1-1(e'' \leftarrow e'')$ bands the $S_1 \leftarrow S_0$ REMPI spectrum also shows the significantly weaker $2-1(e' \leftarrow e'')$, $3-0(a_1'' \leftarrow a_1')$, and $4-1(e' \leftarrow e'')$ transitions (due to weak torsional electronic coupling). ZEKE spectra of toluene through different intermediate resonances of S_1 are presented in Figure 28. The transition frequencies, referred to the respective origin, of the transitions into torsional states of the toluene cation (0, 15, 54, and 75 cm^{-1}) are not very different from those for $S_1 \leftarrow S_0$ (0, 15, 55, and 77 cm^{-1}). This leads to the conclusion that the torsional barriers in the cation and in S_1 are quite similar. An additional band at about 45 cm^{-1} was, however, observed in the cation.

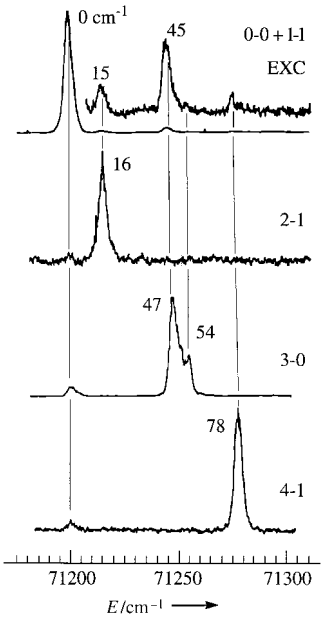

Figure 28. ZEKE spectra of toluene near the origin of the cation ground state $\tilde{X}^{+2}A_2''$ through different rotor states in S_1 (see Figure 27).[111] EXC denotes the $S_1 \leftarrow S_0$ torsional transition used.

For $2e'$ excitation of S_1, a weak ZEKE band at 0 cm^{-1} (assigned as $1e'' \leftarrow 2e'$) and a stronger band at 16 cm^{-1} ($2e' \leftarrow 2e'$) was observed. For $4e'$ excitation, a weak ZEKE band at 0 cm^{-1} ($1e'' \leftarrow 4e'$) and a strong band at 78 cm^{-1} ($4e' \leftarrow 4e'$) occurs. For excitation of the $3a_1''$ level, one observes a weak ZEKE band at 0 cm^{-1} ($0a_1' \leftarrow 3a_1''$), a strong band at 47 cm^{-1} (tentatively assigned as $3a_1'' \leftarrow 3a_1''$), and a moderately strong band (about 30 % of the intensity of the strongest band) at 54 cm^{-1} (tentatively assigned as $3a_2'' \leftarrow 3a_1''$). For ionization through the ground torsional level $0a_1'$ level of S_1, the band at 47 cm^{-1} is much more intense than that at 54 cm^{-1}.

Under the assumption that coupling between torsion and electronic motion makes $a_2 \leftrightarrow a_1$ torsional transitions allowed but not $a \leftrightarrow e$ transitions and based on the fact that the band at 47 cm^{-1} is three times more intense than that at 54 cm^{-1} for ionization through the $3a_1''$ state of S_1, the band at 47 cm^{-1} is assigned to the $3a_1'' \leftarrow 3a_1''$ transition and the band at 54 cm^{-1} to the $3a_2'' \leftarrow 3a_1''$ transition. These assignments of symmetry-forbidden transitions in the ZEKE spectra constitute a major step in understanding motions of large amplitude and the role of torsional-electronic couplings.

5.2. Torsional Motion in the Tolane Cation

The (1+1′) REMPI ZEKE spectrum of tolane was recorded between 63500 and 66500 cm^{-1} by Okuyama et al.[112] Figure 29 shows the comparison of the ZEKE spectra through the different intermediate torsional levels (T^n) of the $S_1\ ^1B_{1u}$ state with zero (T^0), two (T^2), and four quanta (T^4). For the origin excited in the S_1 state (Figure 29a) the origin peak of

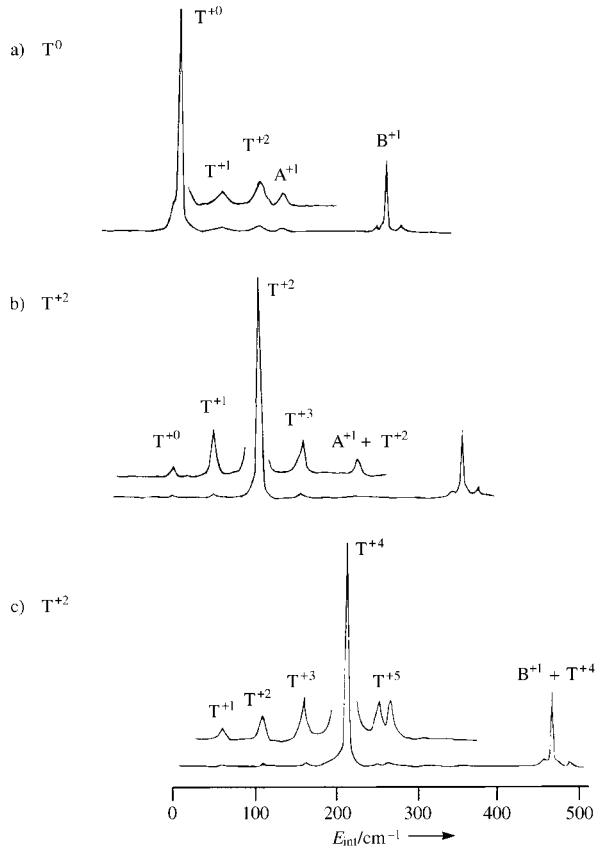

Figure 29. (1+1′) ZEKE spectra of tolane obtained through the a) T^0, b) T^2, and c) T^4 levels of the $S_1\,^1B_{1u}$ state.[112] T = torsional vibration.

the cation dominates along with the totally symmetric vibration B^{+1}. However, there is a signal of lower intensity for the torsional motions with odd quantum numbers (denoted T^{+1}) and even-numbered overtone (T^{+2}). For excitation of two quanta of the torsion S_1 similar results were found (Figure 29b). The strongest transition applies to $\Delta v = 0$ (in this case to T^{+2}). Also the B^{+1} vibration is found in combination with the T^{+2} torsional overtone. Though much less intense, peaks are also found for the cation origin (T^{+0}, symmetry-allowed) with transitions with odd torsional quantum numbers in the ion (T^{+1} and T^{+3}, symmetry-forbidden). A similar observation is made for excitation of the fourth torsional overtone in S_1 where again the $\Delta v = 0$ transition is favored, but torsional overtones with odd quantum numbers (i.e., symmetry-forbidden transitions) are once again observed.

Odd quantum levels of the torsional mode are clearly observed with weak intensities, as seen in Figure 29. Under the D_{2h} point group the torsional mode has a_u symmetry. There is no evidence for a large structural change upon photoionization. Though the intensity of the symmetry-forbidden transitions with odd torsional quantum numbers is weak, these transitions are a clear manifestation of the violation of the Frank–Condon principle. Similar observations have been made for a number of other molecules studied by ZEKE spectroscopy, and may be considered as a common phenomenon in ionization transitions.

6. Radicals

6.1. Benzyl Radical

The first radical studied by ZEKE spectroscopy was the benzyl radical. The ZEKE spectrum obtained by Weisshaar et al.[113] is reproduced in Figure 30. The vibronic coupling in the intermediate state (the A^1, A^2, and A^3 states arising from vibronic coupling of the $1\,^2A_2 - 2\,^2B_2$ system) allows the

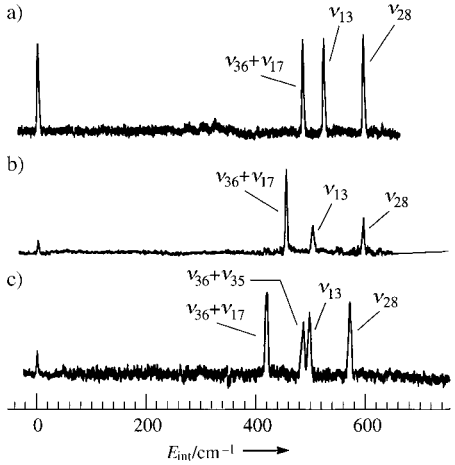

Figure 30. ZEKE spectra of the three isotopomers of benzyl a) (H_7), b) (α-D_2), c) (D_7).[113]

observation of vibrational states of both a_1 and b_1 symmetry (C_{2v} point group) of the benzyl cation in the ZEKE spectrum. The frequencies of the out-of-plane modes of the benzyl cation, obtained from combination bands and ab initio calculations, show that the bond between the exocyclic CH_2 group and the benzene ring has substantially more double-bond character in the ion than in the neutral molecule. The ZEKE spectra for the three isotopomers of benzyl (H_7, α-D_2, and D_7) provide the adiabatic ionization energies $58\,465 \pm 5$, $58\,410 \pm$, and $58\,382 \pm 5$ cm^{-1}, respectively. The observation of both transitions, $\nu_{13}(a_1)$ and $\nu_{28}(b_1)$, is direct evidence of vibronic mixing in the A^1, A^2, and A^3 states and indicates that both electronic components of the $1\,^2A_2 - 2\,^2B_2$ system are detected in the ZEKE spectrum.

6.2. Methyl Radical

The planar methyl radical, isolectronic with NH_3^+, was studied by White, Chen et al.[114] This effort provided the first rotationally resolved ZEKE measurement of a polyatomic radical. One-photon ionization was achieved by using a tunable VUV laser source. The ZEKE spectrum of the methyl radical is reproduced in Figure 31. The rotational structure is very similar to that observed in parallel ($\Delta K = 0$) transitions between bound electronic states in CH_3 and CD_3 radicals; there is little evidence for $\Delta K = \pm 1$ subbands. Under the assumption that mainly P, R, and Q branches contribute to the spectrum, the simulation (Figure 31, bottom) fits reasonably well with the experimental ZEKE spectrum. The

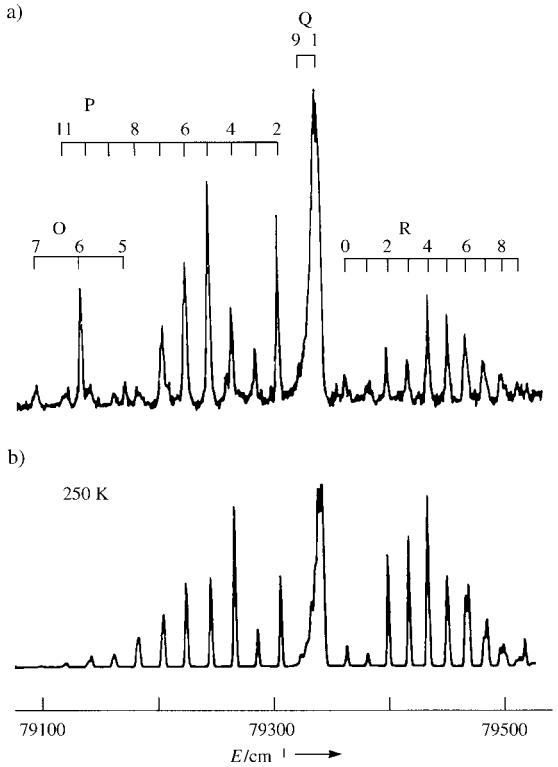

Figure 31. a) Measured and b) simulated one-photon rotationally resolved ZEKE spectra of the methyl radical with assignment of O, P, Q, and R transitions.[114]

exclusive presence of the $\Delta K = 0$ transition suggests that only the ka_1' continua account for the transitions. This seems to be in disagreement with the analysis of the Rydberg series.

7. Hydrogen-Bonded Clusters

Hydrogen bonding has received enormous attention over the years owing to its ubiquity in biological systems.[115] The detailed study of hydrogen bonding in such systems is not straightforward, however, and attention has been focused on smaller systems in environments that are more amenable to interpretation by the chemist. The biggest successes have come from the study of 1:1 complexes in molecular beams.[116,117] Although numerous studies have been performed on neutral complexes, there are very few studies that have concentrated on ionic species. These species are of great importance, as fundamental processes such as solvation depend on the interaction of ionic species with neutral molecules. The paucity of such studies is a result of the difficulty of producing significant quantities of ionic complexes in the gas phase (although infrared spectroscopy of ions is an extremely active field[118–120]). Conventional PES does not offer sufficient resolution to determine the soft intermolecular vibrations, as can be seen in Figure 32 for phenol, phenol–water and phenol–$(water)_n$.

The major study of hydrogen-bonded species with ZEKE spectroscopy took place in one of our laboratories in the mid 1990s. To date, five different hydrogen-bonded species have been studied, all containing phenol as the proton-donating moiety: phenol–water ($PhOH-H_2O$),[40–42,121] phenol–methanol ($PhOH-MeOH$),[43] phenol–ethanol ($PhOH-EtOH$),[44] the phenol dimer ($PhOH-PhOH$),[45] and phenol–dimethyl ether ($PhOH-DME$).[46] The hydrogen-bonded clusters discussed here were recently reviewed in a broader context.[18] The experimental modifications used to study $PhOH-H_2O$ are discussed in detail in the above-mentioned ZEKE studies. Briefly, phenol (heated up to 100 °C) and water vapor (partial pressure 10–50 mbar) were expanded through a 300μm nozzle into a vacuum chamber with up to 6 bar of argon or neon as carrier gas to produce the $PhOH-H_2O$ complex. To record a ZEKE spectrum, the first dye laser was fixed resonant with the S_1 intermediate state of the complex, while the second dye laser was scanned through the ionization thresholds to populate the ZEKE Rydberg states; these were subsequently field-ionized by a delayed extraction pulse of 0.7 $V\,cm^{-1}$ (delay 2 μs).

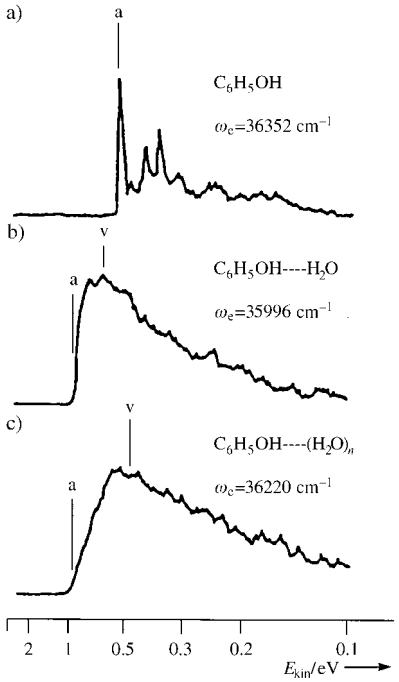

Figure 32. Photoelectron spectra of a) phenol, b) phenol–water, and c) higher pheno–water clusters through the S_1 intermediate state.[127].

7.1. Phenol–Water

The $PhOH-H_2O$ complex and the series of complexes $PhOH-(H_2O)_n$ ($n = 1-4$) have received much attention over the last 10–15 years. Several experimental techniques have been employed (see reference [18] for a comprehensive review). A number of ab initio studies on the neutral electronic ground state have also been published,[122–125] all of which agree that the water lies perpendicular to the plane of the phenol and that the water hydrogen atoms are symmetric with respect to the mirror plane of the phenol ring; the complex is thus C_s-symmetric. Experimental studies on the 1:1 complex have concentrated on the first excited

singlet state S_1 (formed by a $\pi^* \leftarrow \pi$ excitation of the phenol ring) in the main, although some information is available on the ground state S_0. The (1+1′) REMPI spectrum of the PhOH – H_2O complex shows only a meager degree of structure.[126] The transition into the vibrationless state is the most intense, suggesting that the geometries of the S_1 and S_0 states are fairly similar—at least along the hydrogen-bonding coordinates. Two other intermolecular vibrations appear: the reasonably strong stretching vibration (σ) at 156 cm^{-1} and the weak in-plane wagging vibration (γ') at 121 cm^{-1}. The assignments of these bands have been refined over the years and can now be considered as certain, as shown by comparison of a high-quality (1+1′) REMPI spectrum of the PhOH – H_2O complex with ab initio calculations.[42,122,130]

Information about the low-frequency intermolecular vibrations of the ionic complex, in contrast to the neutral states of the 1:1 PhOH – H_2O complex, was rather sparse before the ZEKE studies.[40–42,121] A conventional (one-color, two-photon) time-of-flight photoelectron spectrum (REMPI-PES)[127] measured through the vibrationless S_1 state does not show resolved structure for the vibrations of greatest interest, the intermolecular modes (see Figure 32). Two-color photoionization efficiency (REMPI-PIE)[128] measurements through the vibrationless S_1 origin and the S_1 level, excited with one quantum of the intermolecular stretching vibration, showed the presence of at least one intermolecular vibration as a progression of steps in the ion-yield spectra. This vibration at 242 cm^{-1} was assigned to the intermolecular stretching mode of the ionic complex. However, none of the other five possible intermolecular modes were observed.

In 1994 the 1:1 PhOH – H_2O complex was investigated in a more complete ZEKE spectroscopic study[42] that included the triply deuterated complex (in which all oxygen-bound hydrogen atoms were substituted by deuterium atoms). For the non-deuterated complex, ZEKE spectra were obtained by exciting through three intermediate vibronic states ($S_1 0^0$, $S_1 \sigma^1$, and $S_1 \gamma'^1$; Figure 33). From the ZEKE spectra, the field-free ionization energy (corrected for the extraction field) was determined to be $E_i = 64027 \pm 4$ cm^{-1}. The same value, within experimental error, was obtained from all three intermediate states. The ionization energy of the fully protonated complex is 4601 ± 8 cm^{-1} lower than that of the isolated phenol molecule[129] (68628 ± 4 cm^{-1}). In a further work the partially deuterated (d_1) – (d_3) complexes were investigated.[121]

From recent work, five out of the six possible intermolecular vibrations were extracted. As noted above, the predominant feature is the progression of the intermolecular stretching vibrations, which is also seen in combination with other intermolecular modes. This long progression (consisting of five quanta) of the intermolecular stretching vibration is indicative of the expected large change in the length of the hydrogen bond upon ionization. It is interesting that this progression is so strong (it is also observed in photoionization efficiency measurements),[128] and a decrease in bond length of 0.018 Å was estimated from a one-dimensional Franck – Condon calculation. The progression itself was found to be quite anharmonic, a general finding from the ZEKE spectra of the different hydrogen-bonded complexes. The increase in frequency of the intermolecular stretching vibration of the

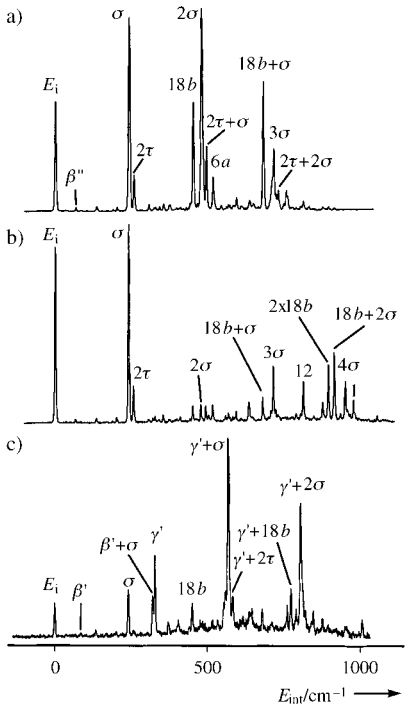

Figure 33. ZEKE spectrum of phenol – water a) through the vibrational origin of S_1 state (0^0), b) through the intermolecular stretching vibration excited in the S_1 state (σ^1), and c) through the intermolecular in-plane wagging excited in the S_1 state (γ').[42]

cation (240 cm^{-1}) over that in the S_1 state (157 cm^{-1})[42] and the S_0 state (155 cm^{-1})[122] illustrates the large increase in binding energy upon ionization. The other intermolecular vibrations that were observed are for out-of-plane bending (β'') at 67 cm^{-1}, in-plane bending (β') at 84 cm^{-1}, the first overtone of the torsional mode (2τ) at 257 cm^{-1}, and in-plane wagging (γ') at 328 cm^{-1}. Various features of the spectra were used to assign these modes, including the magnitude of shifts in vibrational frequency on deuteration, comparison with ab initio calculations[125] that were carried out concurrently, and observation of the changes in intensity as the intermediate S_1 vibronic level was changed. The latter point was supported by Figure 33: In the ZEKE spectrum through the intermolecular $S_1 \gamma'^1$ level (Figure 33c) the ionic intermolecular in-plane wagging (γ') is strongly enhanced (as is the progression of the intermolecular stretching vibration starting on that particular vibrational origin) compared to the other two ZEKE spectra through the $S_1 \sigma^1$ (Figure 33b) and S_1 origin level (Figure 33a). The sixth intermolecular vibration, the out-of-plane wagging γ'' at 261 cm^{-1}, has now been identified from a ZEKE spectrum through the intermediate S_1 state (145 cm^{-1}).[130]

One final point of interest is that the intramolecular ν_{18b} vibration of the complex at 450 cm^{-1} couples strongly with the intermolecular stretching vibration. This observation was used to explain why this vibration appeared so prominently in the ZEKE spectrum of this complex, while it was seen only weakly in the ZEKE spectrum of the isolated phenol molecule. The coupling was identified from normal-mode pictures obtained from the ab initio calculations[125] of the frequencies.

7.2. Phenol – Methanol

The study of the PhOH – MeOH complex was carried out in a similar way as the PhOH – H_2O complex: Phenol was heated, and the resulting vapor and methanol (partial pressure 20 – 100 mbar) were expanded with argon (up to 6 bar). The (1+1′) REMPI spectrum was difficult to interpret owing to the proximity of a number of vibrations.[18] Vibrational levels in the S_1 state were used as intermediate states on the way to ionization. The ZEKE spectrum[43] obtained by exciting through the S_1 vibrationless level is particularly striking (Figure 34), as progressions of about ten quanta of a

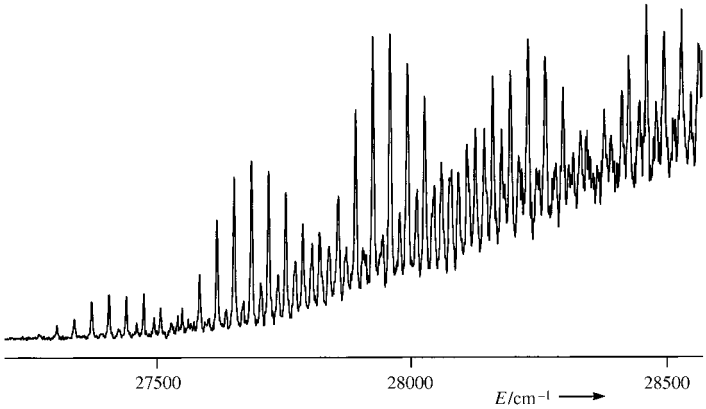

Figure 34. ZEKE spectrum of phenol – methanol through the vibrational origin of $S_1 0^0$.[43]

low-frequency vibrational mode, η_1,[131] of 34 cm^{-1} appear in combination with components of an anharmonic progression of the intermolecular stretching vibration of 278 cm^{-1}. This pattern clearly suggests a rather substantial change in geometry upon ionization. The adiabatic ionization energy was determined to be 63 207 ± 4 cm^{-1} (field-free value), which represented a large increase in bonding energy of 5421 ± 8 cm^{-1} over that in the S_0 state. This is exemplified by the large increase in the intermolecular stretching vibration over the values of 176 cm^{-1} in the S_1 state[43] and 162 cm^{-1} in the S_0 state obtained by dispersed fluorescence spectroscopy.[132] Additionally, another set of progressions of the intermolecular mode of 34 cm^{-1} was seen between the latter components, this time in combination with a third intermolecular mode of 52 cm^{-1}. The ZEKE spectrum obtained through the S_1 state which was excited with one quantum of the lowest frequency intermolecular mode showed the same vibrations, but with a substantially changed Franck – Condon envelope. This allowed the identification of a fourth intermolecular mode, η_4, at 153 cm^{-1}. A slightly different envelope of the vibration at 34 cm^{-1} was also obtained when exciting through the S_1 state with one quantum of the intermolecular stretching vibration (σ). The other two intermolecular modes of the PhOH – MeOH cationic complex were identified from the ZEKE spectrum obtained through a combination band; their values were 76 and 158 cm^{-1}. Therefore, as for PhOH – H_2O, in PhOH – MeOH all six intermolecular modes of the cationic complex were identified by using different intermolecular vibrational S_1 levels as intermediate resonances.

8. van der Waals Complexes

The first ZEKE study of a van der Waals complex was carried out by Chewter et al.[133] on the benzene – argon cluster. The ZEKE spectrum revealed only one peak, assigned to the ionization threshold, that was shifted with respect to the benzene origin by 172 cm^{-1}. From that spectrum and the rather small change in ionization energy compared to the benzene monomer, the conclusion was drawn that ionization of the complex does not lead to a drastic increase in the binding energy of the argon atom.

For complexes containing benzene derivatives, an extensive ZEKE study of aniline – Ar and aniline – Ar_2 was carried out by Knee et al.[134] The ZEKE spectra they measured (Figure 35 were normalized with respect to the origin of the

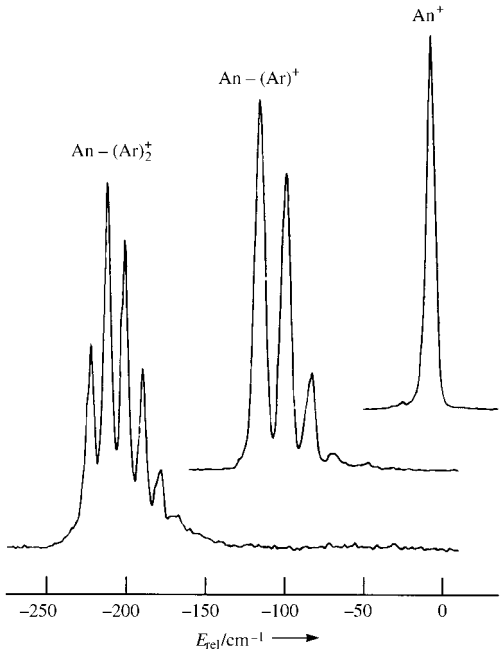

Figure 35. ZEKE spectrum of aniline – argon (An – Ar) complexes at the ionization threshold (with respect to the aniline cation).[134]

aniline ion. For aniline – Ar the ionization energy was determined to be 62 168 ± 4 cm^{-1}, indicating that the cation is more tightly bound than the S_0 and S_1 states by 113 and 60 cm^{-1}, respectively. From a comparison of the ZEKE spectrum of aniline – Ar and the $S_1 \leftarrow S_0$ transition in the neutral molecule, as investigated by Bieske et al.,[135] it is apparent that the ZEKE spectrum shows more pronounced vibrational structure, specifically a progression of 15 cm^{-1} for a single vibration. The analysis of the intermolecular van der Waals modes for the $S_1 \leftarrow S_0$ transition led to the following classification: symmetric stretching s_z (49 cm^{-1}), symmetric bending b_x (22 cm^{-1}), and asymmetric bending b_y (19 cm^{-1}). The motion of argon along the C_2 rotation axis (in C_{2v}-symmetric aniline) corresponds to the symmetric bending. The asymmetric bending motion takes place across the aromatic plane perpendicular to the C_2 axis. Fundamentals and overtones of these two symmetric modes are allowed and have been observed in the S_1 spectrum; however, they are not

very intense, indicating only a slight change in geometry upon $S_1 \leftarrow S_0$ excitation. By comparison with the S_1 spectrum, Knee et al. assigned the mode at 15 cm^{-1} as the symmetric bending vibration in the cation. The relatively long progression observed, according to Franck – Condon arguments, indicates a significant change in the geometry along the coordinations of symmetric bending upon ionization. This was explained by a positive charge on the nitrogen atom, which shifts the equilibrium position of the argon towards the amino group. No ab initio calculations were to support the assignment.

For aniline – Ar_2 a shift of 220 cm^{-1} relative to S_0 and 113 cm^{-1} relative to S_1, with an ionization energy of 62 061 ± 4 cm^{-1}, was obtained. The change in bond energy is almost exactly twice that of the 1:1 complex, producing a considerably extended Franck – Condon envelope. The most intense peak within the vibrational van der Waals progression is not found at the ion origin, but at the second member of the mode at 11 cm^{-1}. Following the symmetry analysis of Bieske et al.[135] for the S_1 spectrum of aniline – Ar_2 and their classification, the progression observed in the ZEKE spectrum was assigned to the symmetric bending vibration along the C_{2v} axis (b_x). This vibration has a frequency of 15 cm^{-1} in the S_1 state, and upon ionization a reduction in frequency is again observed.

8.1. Transfer of Vibrational Energy and Predissociation in S_1

The excitation of an intramolecular vibration (i.e., in the aniline manifold) can lead to dissociation of the aniline – Ar complex due to the transfer of the intramolecular vibration energy to translational energy.[136] A potential scheme to probe such S_1 dynamics is shown in, Figure 36. The pump

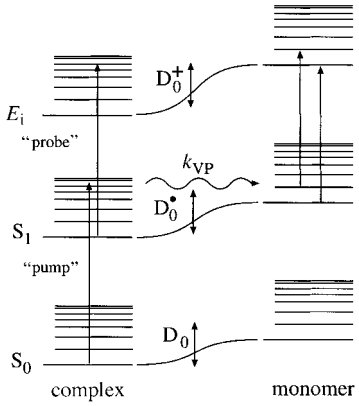

Figure 36. Schematic energy diagram for intramolecular energy redistribution and dissociation in a van der Waals cluster. D_0 = dissociation energy.

photon excites an intramolecular vibration in the S_1 state of the neutral van der Waals molecule. The ionization rate due to the probe laser (ionization laser) then has to compete with the predissociation rate (rate constant k_{VP}). Depending on the timescale of the experiment (i.e., the delay between pump and probe laser) one observes either the vibrations due to the aniline – Ar van der Waals complex or the aniline ion in the ZEKE spectrum. For small delay times (i.e., the time overlap of pump and probe laser) one expects mainly ionization into the stable van der Waals cluster, whereas vibrations of the monomer cation are observed for longer delays.

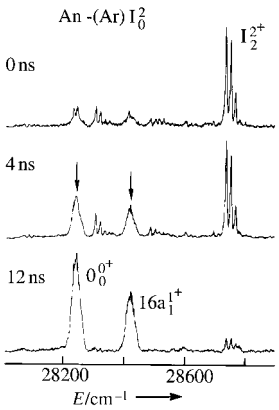

Figure 37. ZEKE spectrum of aniline – argon through the $S_1 I_0^2$ level (762 cm^{-1}; i.e., ca. 300 cm^{-1} above the dissociation energy of the S_1 state) of the complex as a function of the delay time between pump and probe laser.[136] The arrows indicate product states of the aniline monomer which grow in with increasing probe delay time and which are a measure of the dynamics in the S_1 state (dissociation and intervibrational redistribution).

Excitation of the overtone of the inversion vibration in the aniline ring (denoted I) is of particular interest. The first overtone of this vibration is clearly seen in the $S_1 \leftarrow S_0$ transition at 762 cm^{-1}. Excitation of this vibration should considerably interfere with the movement of the argon atom sitting on the aniline ring. When pumping the I_o^2 transition, the ZEKE spectrum indeed reveals features that are attributed to both the reactant (aniline – Ar) and the product (aniline). Figure 37 reproduces the ZEKE spectra for different probe laser delay times (with respect to the pump laser). Closer inspection reveals that when both pump and probe laser overlap in time, the spectral features observed are mainly due to the van der Waals aniline – Ar complex. With increasing delay time, features due to the van der Waals complex decrease in intensit, and vibrational features due to the monomer appear (see the arrows in Figure 37) and become prominent at delay times of 4 and 12 ns. Taking into account the energetics, the measured $S_1 \leftarrow S_0$ excitation spectra, and ZEKE spectra of the aniline monomer, Knee et al.[134] were able to assign these vibrational features in the ZEKE spectrum with an optical delay of 12 ns to the transition into the origin of the aniline cation (denoted 0_0^{0+}) and the transition from the ν_{16a} vibration in which one quantum is excited into the ion that is also excited with one quantum of ν_{16a} (denoted $16a_1^{1+}$). Therefore, these spectra lead to the conclusion that the predissociation channel can leave the monomer either vibrationless or excited with one quantum of the ν_{16a} mode. The peaks attributed to the monomer are much broader than the ZEKE peaks not subject to predissociation. The width of approximately 28 cm^{-1} was attributed to rotational excitation of the monomer produced in the S_1 state by dissociation.

9. Mass-Analyzed ZEKE Measurements

The PFI of ZEKE Rydberg states results in the formation of an electron and a cation, which may also be detected by mass analyzed threshold ionization (MATI); this mass-selective technique was originally suggested by Johnson et al.[137] Compared to detection of the electron, which is very easy, that of cations must take place in the presence of other

spontaneous ions and is considerably more difficult. Hence, for normal ZEKE spectroscopy electron detection is more suitable, but MATI clearly offers additional information about mass. Optimized detection schemes are described in references [23–25].

The advantages of combining mass detection with ZEKE spectroscopy are particularly apparent for systems undergoing dissociation. An experiment by Krause and Neusser [138,139] gave the following results for the dissociation of the C_6H_6-Ar van der Waals complex (the frequency of the first laser was tuned to the intermediate state of the C_6H_6-Ar complex produced in the seeded supersonic jet): The 6_0^1 transition is red-shifted by 21 cm^{-1} from the corresponding transition in benzene. Under these conditions the selectivity of excitation of the intermediate state is very good, and it is possible to ionize only the C_6H_6-Ar complex. The threshold ion, $[C_6H_6-Ar]^+$ and the fragment $C_6H_6^+$ were detected; the resulting mass-selected ZEKE spectra are shown in Figure 38. The spectrum in Figure c was obtained by selecting mass 78 u for a photon energy in resonance with the 6^1 state of benzene; it shows the vibronic structure of the monomer benzene cation.

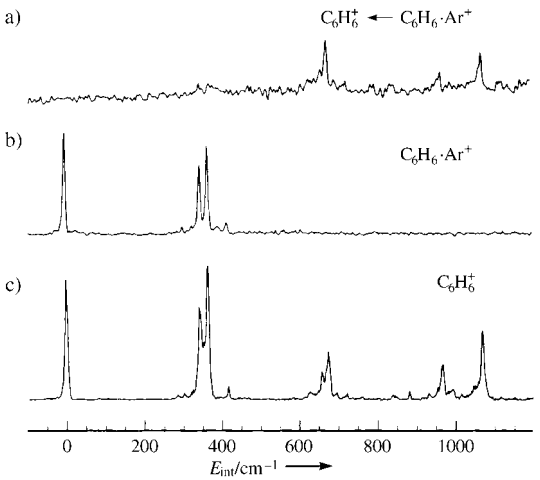

Figure 38. Mass-resolved ZEKE spectra in three different mass channels. a) ZEKE spectrum of benzene–argon measured in the benzene mass channel (78 u). The benzene ions are produced by PFI of fragment ZEKE Rydberg states of benzene originating from fragmentation of the benzene–argon complex.[138] b) ZEKE spectrum of benzene–argon through the $S_1 6^1$ intermediate state, measured by detecting benzene cations produced from PFI of ZEKE Rydberg states of benzene–argon (118 u). c) ZEKE spectrum of the benzene monomer through the $S_1 6^1$ intermediate state, measured by detecting benzene cation produced from PFI of ZEKE Rydberg states of benzene (78 u).

Figure 38b shows the corresponding ZEKE spectrum for which mass 118 u was selected and the photon energy is in resonance with the 6^1 intermediate state of the neutral C_6H_6-Ar van der Waals complex. The resulting ZEKE spectrum is red-shifted by 127 cm^{-1} with respect to ZEKE spectrum of benzene due to the increased binding energy in the ion compared to the neutral molecule. A comparison of the ZEKE spectra of C_6H_6-Ar and benzene clearly shows that vibrational states above the 4^1 vibronic state have disappeared in the former. Those higher energy vibrations that disappeared in the ZEKE spectrum for mass 118 u appear in the ZEKE spectrum at mass 78 u (Figure 38a), which originates from the dissociation of $[C_6H_6-Ar]^+$ since the intermediate state of the neutral cluster is pumped and selected in the experiment. The experimental finding that the spectral signature of the cluster cation is actually found for the mass of the fragment (daughter ion) is quite astonishing. The dissociation of $[C_6H_6-Ar]^+$ by evaporation of the argon atom occurs within less than 100 μs and at an internal energy lower than 629 cm^{-1} (position of $16^1 6^1 \pm 3/2$).

This leads to the striking conclusion that the electron in the ZEKE Rydberg state does not notice dissociative processes in the ion core since it is bound by the positive Coulombic charge of the ion core. Higher multipole moments and even dissociative dynamics of the core do not constitute a sufficient perturbation to eject the ZEKE Rydberg electron. Hence, after the dissociation process of the core the ZEKE Rydberg electron is still bound by the positive charge now sitting on the fragment daughter ion. When a pulse field is applied this electron can be removed to produce an ion, and this ion is subsequently separated and measured in the MATI experiment. Similar results were also observed in the *p*-DFB–Ar system.[140] These measurements allow the determination of the lower and upper limits for the dissociation energy. In an additional study on benzene–krypton this dissociation energy could be determined within narrower ranges, and a comparison to the most advanced theoretical predictions could be made.[141,142]

Much higher dissociation energies were reached in an experiment in which benzene ZEKE Rydberg states[143] were excited about 4 eV above the ionization limit, leading to strong fragmentation.[144] In spite of the high translational energy of the fragments, it was clearly established that the Rydberg electron once again follows the ionic core of the fragment. The ZEKE Rydberg state of the daughter fragment, with the fragment ion core, was then pulsed-field ionized in these mass-resolved ZEKE experiments.[145] This result came as a big surprise and will have important implications for experimental studies of the dynamics of reaction in which fragments are "parked" in long-lived ZEKE Rydberg states.

MATI experiments on the $PhOH-H_2O-Ar$ complex, which shows hydrogen van der Waals bonds, should prove interesting for studying the interplay between different types of intermolecular bonds during fragmentation. Rapid intervibrational redistribution (IVR) of vibrational energy initially localized at the intermolecular hydrogen bond into the weaker van der Waals bond has already been observed in this system,[146] leading to dissociation of the weaker van der Waals bond. The photoionization efficiency (PIE) curve for $[PhOH-H_2O-Ar]^+$ displays steps that correlate to each strong peak in the PFI-ZEKE spectrum. Notably, the steps in the PIE spectrum are rather broadened since the low-frequency intermolecular van der Waals vibrations of the argon atom and their combinations with the equally low-frequency vibrations of the hydrogen bond produce a high density of vibrational states close to each ionization threshold. Above a certain photoionization energy, the intensity of the $[PhOH-H_2O-Ar]^+$ signal remains constant,

while that of the $[PhOH-H_2O]^+$ signal increases, reflecting fragmentation of the parent cluster by ejection of argon. The energy difference between the appearance potential becomes constant in the $[PhOH-H_2O]^+$ channel and the point at which the $[Ph-H_2O-Ar]^+$ signal provides an upper limit for the dissociation energy of $[PhOH-H_2O-Ar]^+$ to $[PhOH-H_2O]^+$. This value should be reasonably close to the true dissociation energy as the density of optically accessible vibrational states close to the dissociation threshold is high.[146]

10. Metals, Metal Oxides, and Metal–Carbide Clusters

A new field that has developed over recent years is the application of ZEKE spectroscopy to metal carbides and metal oxides. Analogous systems are believed to play a vital role in catalysis, and it is of great interest to prepare these compounds in a mass-selected way to study their structure and potentially their reactivity as a function of known composition.

Németh et al.[147] obtained a well-resolved ZEKE spectrum of the silver dimer and thus improved values for the vibrational frequencies and ionization. More importantly, the ZEKE spectrum of Ag_2 revealed excitation in the cation up to very high vibrational quantum numbers ($\nu^+ = 10$). This completely non-Franck–Condon vibrational envelope was interpreted by channel couplings of the ZEKE Rydberg states with high n with those with low n. This results in anomalous intensities for the transitions that are forbidden by Franck–Condon rules.[148]

Small vanadium, niobium, and yttrium clusters were studied by Yang et al.[149–151] For the vanadium dimer, transitions were observed from the A state to two spin-orbit components with $\Omega = 1/2$ and $\Omega = 3/2$[150,151] confirming that the cation ground state has $^4\Sigma_g^-$ symmetry, in accordance with previous experimental and theoretical work. For the rotational distributions in the $^4\Sigma_g^- \leftarrow A^3\Pi_{1u}$ and $^4\Sigma_g^- \leftarrow A^3\Pi_{2u}$ transitions striking differences were observed for the rotational propensity rules. The adiabatic ionization potential was determined to be 51271.1 cm^{-1}.

The metal clusters probed in these experiments were produced by laser ablation of the metal with a supersonic expansion of helium gas over the target from a pulsed beam valve.[149] The clusters were then excited in a two-color experiment. The geometric structures of the niobium and niobium oxide clusters are important (but unsolved) problems in cluster science as models for reactive systems in heterogeneous catalysis. To take full advantage of the cluster-surface analogy it is necessary to establish the structure of metal clusters containing several transition metal atoms, both in the presence and absence of ligands. It has proved difficult to address this problem in a satisfactory way with conventional spectroscopic techniques. The dense manifold of vibronic states that exists for even fairly small groupings of transition metal atoms has been a major impediment to the use of most forms of electronic spectroscopy for this purpose.

Given the lack of experimental data on the structure of small transition metal clusters, one often has to rely on geometries determined from electronic-structure calculations. Density functional theory (DFT) calculations and other ab initio techniques have been used; the validity of the different theoretical approaches is under intense, even controversial, discussion. The DFT results presented by Yang et al.[149,151] seem quite reasonable considering the difficulties encountered in such systems. It would be interesting if it can provide structures for transition metal clusters containing up to seven or eight atoms and bond lengths, including those for metal–ligand and metal–metal bonds.

The structures of transition metal systems can therefore be elucidated with a combination of ZEKE spectroscopy and ab initio calculations. This is a very promising development since it would allow ab initio calculations for large chemical systems. For Nb_3O the ground electronic configuration of the Nb atom is $4d^4 5s^1$. The electronic structure of a molecule containing three Nb atoms is very complex since the Nb atom has 15 electronic terms below 2 eV. Remarkably, the ZEKE spectrum of Nb_3O[151] (Figure 39) shows a completely resolved

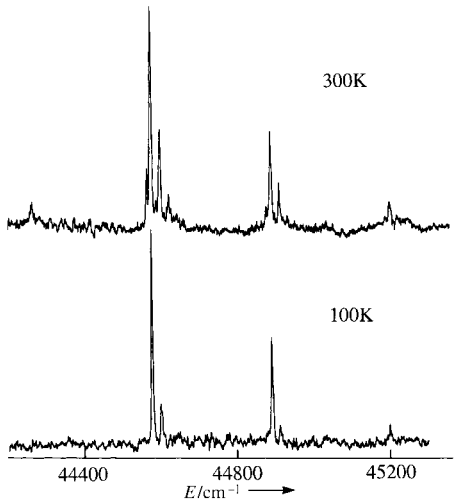

Figure 39. ZEKE spectra of Nb_3O at 300 K and 100 K.[151]

vibrational structure, which can readily be assigned and simulated with multi-dimensional Franck–Condon factors. The Franck–Condon factors were calculated with use of the stable geometries and harmonic frequencies obtained from DFT caluculations for the neutral Nb_3O molecule and the Nb_3O^+ ion. The remarkable agreement between the experimental and simulated ZEKE spectrum establishes the power of the ZEKE approach, coupled with DFT electronic structure and Franck–Condon calculations for resolving questions concerning the structure of these small transition metal clusters.

Figure 40 presents the minimum-energy structures and their relative energies for Nb_3O and Nb_3O^+. These geometries were obtained by minimization of the total energy without symmetry constraints.[151] The most stable structure for both Nb_3O and Nb_3O^+ is planar with C_{2V} symmetry. The oxygen atom is bound with equal bond lengths to two Nb atoms, and there are two distinct Nb–Nb bond distances in the cluster. The observed ZEKE spectra are in perfect agreement with this structure, as indicated by a simulation with the C_{2v}

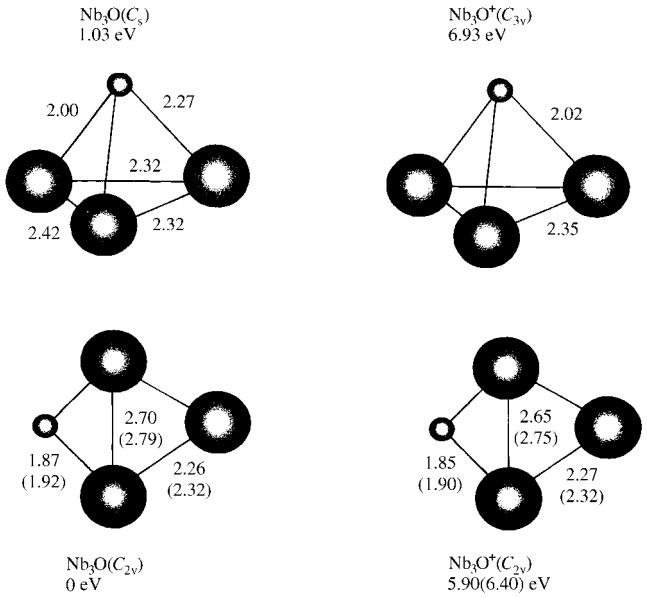

Figure 40. Geometries and relative energies for Nb_3O and Nb_3O^+ calculated with density functional theory.[151]

structure (Figure 41). This confirms that three-dimensional structures like the ones in Figure 40 are associated with excited states, which play no role here.

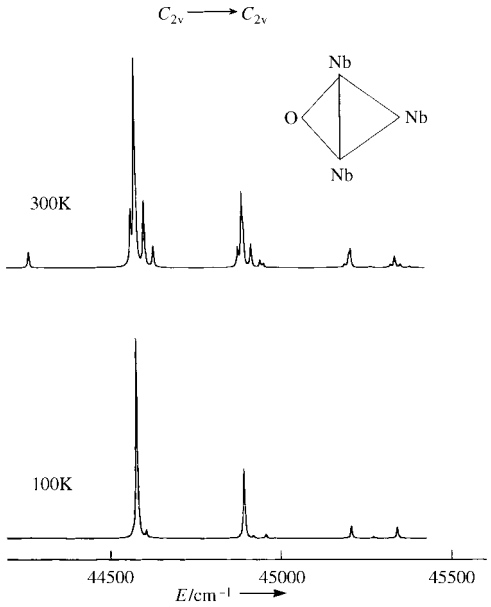

Figure 41. Simulation of the ZEKE spectra shown in Figure 39 with use of the structures shown in Figure 40.[151]

An even richer spectroscopic structure can be seen for the cluster Nb_3C_2. The ZEKE spectrum showing several vibrational progressions is reproduced in Figure 42.[152] For this cluster, again with use of the DFT formalism, agreement was obtained for a C_1 structure of the neutral molecule and a D_{3h} structure for the cation (Figure 43b). The simulation of the ZEKE spectrum, again taking into account a multi-dimensional Franck – Condon approach, is quite reasonable, though not all features of the spectrum appear (Figure 43a).

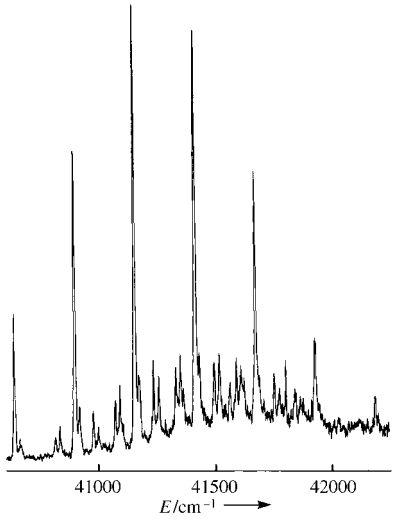

Figure 42. ZEKE spectrum of Nb_3C_2.[152]

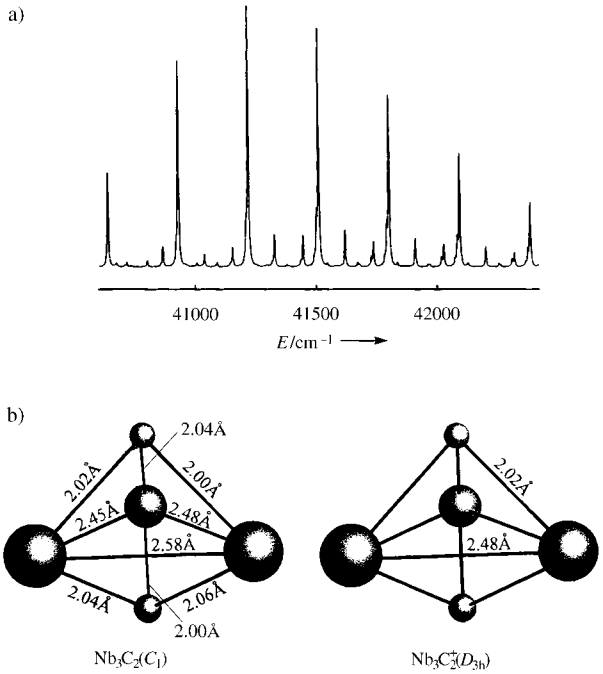

Figure 43. a) Simulated ZEKE spectrum of Nb_3C_2. b) Structures obtained from DFT calculations.[152]

In conclusion, ZEKE spectroscopy combined with the sensible application of a suitable ab initio calculations reveals vibrational information on small transition metal clusters. The quality of the agreement between the experimental and the simulated spectra is sufficient to assign the geometry of a complex transition metal cluster.

11. Anions

The study of anions by ZEKE spectroscopy poses significant problems since the PFI variant of the ZEKE method (see

Figures 5–8) does not quite provide the same improvement (since the requisite Rydberg states do not exist), and electrons are detected just above threshold within a very small energy range (see Figure 4). This, in turn, implies that significantly more care must be taken to shield the ionization region from stray electric and magnetic fields. Neumark et al. first applied the ZEKE method to photodetachment spectroscopy[64] and have been very active in this field. They have successfully performed studies on clusters of germanium,[154] silicon,[155] and halide ion molecules[156,157] as well as transition state complexes.[65] Their first ZEKE photodetachment spectrum was obtained in 1989 for the SH^- anion (Figure 44).[64] It shows the clearly resolved rotational structure of the corresponding neutral molecule, the SH radical. More recently,

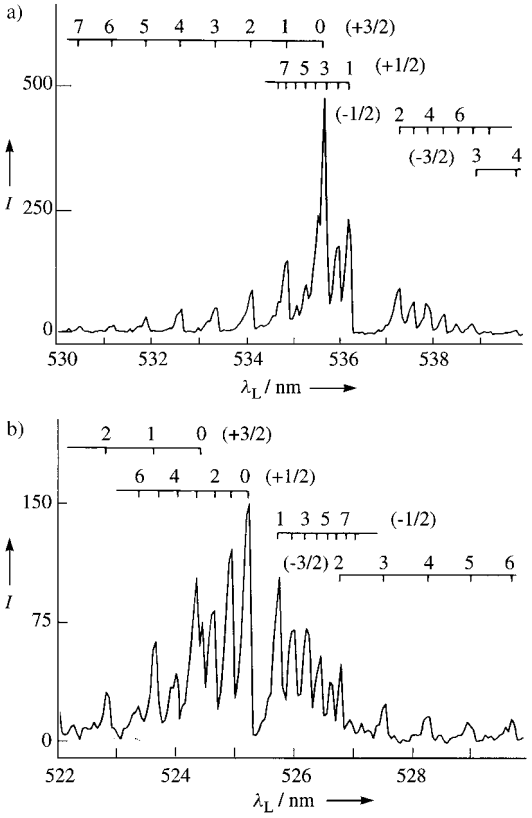

Figure 44. ZEKE photodetachment spectrum of SH^- with rotational resolution for a) $SH(^2\Pi_{3/2}) \leftarrow SH^-(^1\Sigma^+)$ and b) $SH(^2\Pi_{1/2} \leftarrow SH^-(^1\Sigma^+)$. The SH^- J'' values are given; the ΔJ values are in parenthesis.[64]

Bässman et al.[158] constructed a high-resolution ZEKE spectrometer for anions (resolution 1.5 cm^{-1}) and obtained spectra of the $I^- - H_2O$ cluster. The spectra are dominated by two low-frequency modes at 45 and 210 cm^{-1}, which were assigned to the $I-H_2O$ stretching and in-plane bending modes, respectively. The fine structure was tentatively assigned to rotational excitation around the I–O axis. In the future it may be possible to significantly increase the resolution of anion spectra for such complexes between halides and polar molecule by employing novel "dipole-bound" excited states,[159,161] which have recently been discovered in such clusters. Excitation of the complex from the ground state to the weakly bound excited state could be followed by PFI to give an anionic version of ZEKE-PFI.[160]

The other main area of application, to metals and mixed clusters, was first carried out by Ganteför et al.[39,162,163] and further developed by Drechsler et al.[164,165] Photodetachment spectroscopy of anionic clusters is a useful technique, as mass selection of the charged clusters may be achieved. The information gained from the photodetachment spectrum gives direct information on the neutral species.

11.1. Transition States

According to long-standing common belief, it seemed impossible to directly measure the transition state of a chemical reaction. ZEKE spectroscopy, however, has been successfully used for this purpose from a rather different angle than for recent femtosecond pump–probe experiments.

During the hydrogen-exchange reaction $A + HB \rightarrow AH + B$ a transition state is formed in which the hydrogen atom is partway between the A and B molecules.[166] This reaction has been probed by photodetachment of AHB^- complexes by Neumark et al.[167–169] The $ClHCl^-$, $BrHBr^-$, IHI^-, and H_2F^-[170] complexes have been studied by conventional photodetachment spectroscopy. Ab initio calculations were also performed on these species; the work up until the beginning of 1993 has been summarized by Klepeis et al. in their extensive study of the $FHCl^-$ complex.[171] To date, only one experimental study has looked at these complexes with ZEKE spectroscopy, namely, that of Waller et al. on IHI^-.[65] This complex has attracted a significant amount of attention recently, and an ab initio study was performed by Schatz et al.[172]

Weaver et al.[168] looked at the IHI^- and IDI^- complexes in the conventional photodetachment study. One of the stimulations for this investigation was a matrix-isolation study of IHI^- by Ellison and Ault,[173] which indicated that IHI^- was linear and centrosymmetric, as was expected for the transition state of the reaction $I + HI \rightarrow IH + I$. Since calculations had predicted that bound states of the IHI complex existed,[174] it was anticipated that the vertical (most intense) region of the photodetachment spectrum would give direct information on the IHI transition state. A simplified potential for the IHI^- anion and the corresponding neutral molecule is shown in Figure 45. The photoelectron photodetachment spectrum (see

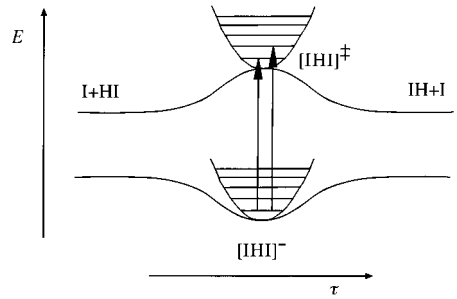

Figure 45. Schematic representation of a part of the [IHI] reaction coordinate with the level structure of the ν_3 vibration in the IHI^- ion and in the activated complex.

Figure 8 including the comparison to the ZEKE spectrum) was obtained by photodetachment of mass-selected anions by the fourth harmonic vibration of a Nd:YAG laser. The resulting electrons were analyzed with respect to their kinetic energy; a spectral resolution of approximately 8 meV was obtained. A series of three peaks was assigned to a progression of double quanta of the asymmetric stretching vibration ν_3.

The simulation of the spectrum indicated that a symmetric stretching vibration quanta should also be associated with each of the transitions in the asymmetric mode, but these were not resolved in this experiment. Owing to the poor spectral resolution, it was not possible to be certain that any of the states of IHI accessed in the photodetachment were bound. The most likely candidate for a bound state was a narrow peak in the spectrum of IDI^-. The ZEKE spectrum[65] (see Figure 8) was more definitive, however, and contained peaks with a width of 30 cm^{-1}. The IHI^- ions were produced and selected as in the previous experiment, but on this occasion they underwent photodetachment by the output of a tunable dye laser; the experimental resolution was between 1 and 2 meV. At this higher resolution, the expected symmetric stretching vibration of the IHI complex was observed for the transitions $\nu_3 = 0$, 2, and 4. They exhibited significantly different widths, which were taken to be indicative of the different lifetimes of the levels in the neutral complex. For example, in the $\nu_3 = 4$ level two components of a symmetric stretching vibrational progression (93 ± 5 cm^{-1}) were observed and assigned to $\nu_1 = 0$ and 1; these spectral widths indicated lifetimes of 180 and 120 fs, respectively. The "hot bands" in the latter feature showed vibrational structure that basically agreed with the data from matrix-isolation experiments.[173] For the $\nu_3 = 2$ feature the peaks were somewhat broader (100 cm^{-1}) and had spacings of about 100 cm^{-1}. In contrast, the $\nu_3 = 0$ level showed a series of peaks whose spacing varied from 160 to 200 cm^{-1} (for higher laser energy). However, this was expected as, calculations had suggested that photodetachment to this level would only access direct-scattering wavefunctions and not quasi-bound levels. Interestingly, comparison of the ZEKE experiment and the calculations showed that only high rotational energy levels of the IHI complex have significant amplitude near the threshold. Also of note is that both a three-dimensional adiabatic model[175] and a recent ab initio calculation[172] indicate a sharp feature at the threshold, which does not appear in the ZEKE spectrum.

11.2. Metallic Clusters

A number of anionic metallic clusters have been studied by Ganteför et al.[161–163] They produced the metal clusters by laser vaporization of a metal target in rare gas jet molecular expansion; the mixture of anions, cations, and neutral moleucles passes through a skimmer. The anions are accelerated, which results in the separation of clusters of different mass. Cluster of a particular mass are then irradiated in a ZEKE photodetachment experiment. The first study looked at the gold dimer and the silver trimer.[161]

For Au_2^- the results showed a progression in the vibrational frequency of the neutral molecule of 146 cm^{-1}. There were also hot bands in the spectrum, which indicate a vibrational frequency as about 188 cm^{-1} for the anionic ground state. The 0–0 band in the ZEKE spectrum was taken as the electron affinity and led to a value of 1.9400 ± 0.0005 eV. An analysis of the Franck–Condon factors led to a vibrational temperature of 165 ± 30 K for the sample gas.

For Ag_3^- only one peak was observed in the ZEKE spectrum.[162] At first sight this may be a little surprising, as the geometry of Ag_3^- is linear whereas Ag_3 is an equilateral triangle. However, there is a linear state of Ag_3 that lies 0.05 eV above the triangular state,[176] and it is detachment to this state that was thought to be responsible for the ZEKE spectrum. The gold hexamer Au_6^- was also studied.[163] The ZEKE spectrum showed a vibrational progression of 107 cm^{-1}, which was also present in the electron total yield spectrum. These studies demonstrate that fundamental information on metal clusters can be quite clearly ascertained from the ZEKE photodetachment spectra. The mass selectivity possible for anions, together with the sensitivity of the ZEKE mothod, combine to provide a powerful tool for gaining information on neutral species which is difficult to obtain by other means.

11.3. Silicon Clusters

The ZEKE spectrum of the Si_3^- complex was acquired by Arnold and Neumark[155] with a resolution of 10 to 15 cm^{-1}. Only the broad, higher energy band (X) gave rise to a ZEKE spectrum. The structure in this spectrum was dominated by a progression with a spacing of 337 cm^{-1}; there were also weaker features and a peak that was red-shifted by 385 cm^{-1} with respect to the origin of the progression at 337 cm^{-1}.

In order to discuss the assignment of the bands, the electronic structure of the Si_3 molecule needed to be considered. The electronic configuration of the first two states (D_{3h} symmetry) is $(1a_1')^2(1e')^4(2a_1')^2(1a_2'')^2(2e')^2$ giving rise to three electronic states: $^3A_2'$, $^1E'$, and $^1A_1'$. The $^1E'$ state is distorted owing to the Jahn–Teller effect and gives rise to two states. The $^1A_1$ and $^1B_2$ states arise from the lifting of the degeneracy of the e′ orbitals into a_1 and b_2 orbitals upon going to C_{2v} symmetry. Under D_{3h} symmetry, the anion has $^2E'$ symmetry and is thus also subject to Jahn–Teller distortion—to a $^2A_1$ and a $^2B_2$ state.

According to QCISD(T) calculations[177] the $^2A_1$ state is the ground state (QCISD(T) = *q*uadratic *c*onfiguration *i*nteraction *s*ingles *d*oubles (*t*riples)). Large calculated differences in the bond angle between the anion and the neutral molecule led Arnold and Neumark to consider the assignment of the vibration at 337 cm^{-1} to the symmetric bending mode ν_2 of the $^1A_1$ state. However, calculations suggested that this assignment could not be correct since the calculated vibrational frequency was far too low; thus, the assignment to the $^3A_2'$ state was favored. QCISD(T) and self-consistent field (SCF) calculations gave a value that was in poor agreement with the measured frequency, whereas values from DFT calculations[178] were in much better agreement. Therefore, band X

was assigned to the $^3A_2' \leftarrow {}^2A_1$ transition, and the progression at 337 cm^{-1} was assigned to the ν_2 vibration of the neutral molecule. Some of the weaker features were assigned to combinations of the ν_2 progression with one quantum of the ν_1 vibration (measured at 501 ± 10 cm^{-1}); other features in the spectrum were assigned to hot band structure. Simulations were then performed to understand the spectrum in more detail. The best agreement was obtained under consideration of the quadratic Jahn–Teller effect, although there were still inconsistencies between the experimental data and calculations.

The conventional photodetachment spectrum of Si_4^- showed a large amount of vibrational structure. Assignment of this spectrum was originally tentative, but recently confirmed by ZEKE spectra and ab initio calculations.[179] Band X did not give rise to any ZEKE intensity, whereas band A gave a rich vibrational structure. Only part of band B and band C gave rise to any ZEKE structure. Band A is shown in Figure 46; it displays additional resolved structure

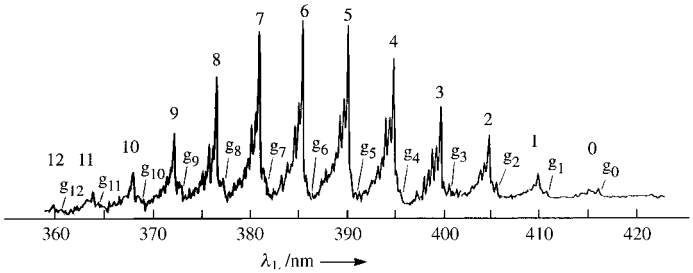

Figure 46. ZEKE photodetachment spectrum of Si_4^- illustrating resolved vibrational structure in band A.[179]

on the individual vibrational components (spacing 312 cm^{-1}). The intensities of the weak features to either side of the most intense feature vary with the conditions of molecular expansion, indicating that they were due to hot bands arising from vibrational excitation in the anion. The weaker features that are blue-shifted with respect to the intense peaks were separated into two progressions of about 50 and 30 cm^{-1}; the two red-shifted features had spacings of about 25 and 53 cm^{-1}. Band A could be assigned to the $^3B_{3u} \leftarrow {}^2B_{2g}$ photodetachment by considering the ab initio calculation[177] with regard to energy and vibrational frequency (the ν_2 mode was calculated to have a harmonic frequency of 306 cm^{-1} for the $^3B_{3u}$ state) as well as expectations based upon the changes in geometry between the neutral and anionic states. Locating the origin of this progression proved difficult owing to the low intensity at the onset of the band. Franck–Condon simulations together with ab initio calculations led to the conclusion that band marked 0 in Figure 46 was indeed the origin of the band. The weak features were assigned by further Franck–Condon calculations and by comparison with the results of ab initio calculations.

Band B′ again showed a main progression (300 ± 6 cm^{-1}) flanked by weaker features. The assignment of this band was based upon the fact that the only state calculated[177] to be in this energy region, and that also could be formed by s-wave photodetachment from the anionic state, was the $^1B_{3u}$ state. The irregular vibrational structure of the weaker features was postulated as being due to vibronic coupling between the electronic states, which were calculated to lie within the range of band A (Figure 46) but that could not be formed by photodetachment of an s wave.

Band C′ was rather broad owing to only partial discrimination of electrons with higher kinetic energy (with a view to increasing the intensity of the rather weak feature). The structure consisted of a progression of about 430 cm^{-1}. The assignment to the $^3B_{1u} \leftarrow {}^2B_{2g}$ photodetachment transition[177] was deemed most likely.

11.4. Metal–Carbide Clusters

As part of a study of catalytically active species, FeC_2^- was studied by Drechsler et al. [164,165] They obtained a very highly resolved ZEKE spectrum, as can be seen from the comparison to the photodetachment photoelectron spectra for excitation at 532 nm and 355 nm (Figure 47). The work gave a greatly improved value for the electron affinity of FeC_2 (15955 cm^{-1}). The vibrational constants associated with the Fe–C vibration were determined to be $\omega_e = 561.6$ cm^{-1} and $\omega_e x_e = 2.1$ cm^{-1}. There was also an indication for another vibration attributed to the C–C vibration at 1975 cm^{-1}. Furthermore, there was evidence of hot bands originating from excitation in the mother anion. The particular significance of these experiments lies in the fact that a resolution of 1.5 cm^{-1} was obtained, the record for ZEKE photodetachment so far.

12. Conclusions

Owing to its unprecedented resolution, ZEKE spectroscopy provides a unique tool for studying a large variety of molecular systems. In this review we have presented some typical examples, mainly focusing on the high-resolution

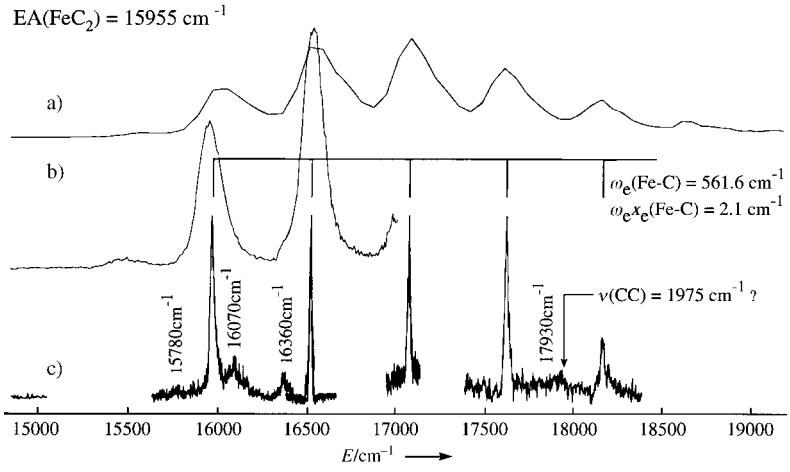

Figure 47. Photodetachment photoelectron spectra (fixed photon energy) of FeC_2^-; a) 355, b) 532 nm. c) ZEKE photodetachment spectrum of FeC_2^-.[164]

spectra of molecular cations that can be obtained by ZEKE spectroscopy. The extension of the technique to free radicals, anions, and thence neutral molecules is still an emerging field. Many laboratories across the world are contributing to the rapid devolpment of this spectroscopy, as documented by four European research conferences at Kreuth in 1991, Giens in 1993, Lenggries in 1995, and Emmetten in 1997. Future experiments will no doubt help to further elucidate the nature of ZEKE Rydberg states and extend applications to anion spectra and neutral molecules. In addition, the method also lends itself to the study of transient species such as radicals or complexes, thus continuing on the lines of the first direct measurements of transition states in chemical reactions.[65] All these initial examples will certainly be followed, as is the case for any emerging spectroscopy, by a rich body of examples, which then forms the broad basis for this new spectroscopy.

Another important chemical aspect concerns the dynamics of hydrogen-bonded clusters. Proton transfer has been probed in such systems by short pulse lasers in the femto- to picosecond regime.[180] The combination of this pump–probe technique with ZEKE detection[181] should be particularly suitable to project out the proton-transfer coordinate[182] from the excited S_1 state of the ion. Combined with mass-selected ZEKE detection, the proton transfer and fragmentation channel of the ion can also be monitored.

In conclusion, one can say that we are standing at the beginning of a rich new spectroscopy which will provide new insights into the chemistry of cations, elusive neutral molecules, and metastable species that are present in reactive mixtures, clusters, van der Waals complexes, and free radicals.

Support from the Deutsche Forschungsgemeinschaft, the Bundesministerium für Bildung, Wissenschaft, Forschung und Technologie, the Fonds der Chemischen Industrie, and the Commission of the European Union is gratefully acknowledged. We are grateful to Dr. Caroline Dessent (York) for careful corrections of the manuscript, and Dipl.-Phys. Franz Hompf (York) and Dipl.-Chem. Wolf-Dietrich Geppert (York) for the German translation. We thank Sabine Mayr (Munich) and John Olive (York) for technical support.

Received: April 24, 1996
Revised version: July 3, 1997 [A 164 IE]
German version: *Angew. Chem.* **1998**, *110*, 1414 – 1444

[1] G. Herzberg, *Electronic Spectra of Polyatomic Molecules*, Van Nostrand, New York, **1966**.
[2] F. I. Vilesov, B. I. Kurbatov, A. N. Terenin, *Sov. Phys. Dokl. Engl. Transl.* **1961**, *6*, 490.
[3] D. W. Turner, M. I. Al Joboury, *J. Chem. Phys.* **1962**, *37*, 3007.
[4] D. W. Turner, C. Baker, A. D. Baker, C. R. Brundle, *Molecular Photoelectron Spectroscopy*, Wiley, London, **1970**.
[5] J. Berkowitz, *Photoabsorption, Photoionization and Photoelectron Spectroscopy*, Academic Press, New York, **1979**.
[6] K. Kimura, S. Katsamuta, Y. Achiba, T. Yamazaki, S. Iwata, *Handbook of HeI—Photoelectron Spectra of Fundamental Organic Molecules*, Japan Science Society Press, Tokyo, **1981**.
[7] P. Baltzer, L. Karlsson, M. Lundqvist, B. Wannberg, *Rev. Sci. Instrum.* **1993**, *64*, 2179.
[8] K. S. Viswanatan, E. Sekreta, E. R. Davidson, J. P. Reilly, *J. Phys. Chem.* **1986**, *90*, 5078.
[9] J. Leahy, K. L. Reid, H. Park, R. Zare, *J. Chem. Phys.* **1992**, *97*, 4948.
[10] L. Åsbrink, *Chem. Phys. Lett.* **1970**, *7*, 549.
[11] A. Niehaus, M. W. Ruf, *Chem. Phys. Lett.* **1971**, *11*, 55.
[12] S. Southworth, C. M. Truesdale, P. H. Kobrin, D. W. Lindle, W. D. Brewer, D. A. Shirley, *J. Chem. Phys.* **1982**, *76*, 143.
[13] K. Müller-Dethlefs, M. Sander, E. W. Schlag, *Z. Naturforsch. A* **1984**, *39*, 1089.
[14] K. Müller-Dethlefs, M. Sander, E. W. Schlag, *Chem. Phys. Lett.* **1984**, *112*, 291.
[15] K. Müller-Dethlefs, E. W. Schlag, *Annu. Rev. Phys. Chem.* **1991**, *42*, 109.
[16] T. G. Wright, G. Reiser, K. Müller-Dethlefs, *Chem. Br.* **1994**, *30*, 128.
[17] I. Fischer, R. Lindner, K. Müller-Dethlefs, *J. Chem. Soc. Faraday Trans.* **1994**, *90*, 2425.
[18] K. Müller-Dethlefs, O. Dopfer, T. G. Wright, *Chem. Rev.* **1994**, *94*, 1845.
[19] *High Resolution Laser Photoionization and Photoelectron Studies* (Eds.: I. Powis, T. Baer, C.-K. Ng), Wiley, Chichester, **1995**.
[20] "High Resolution Spectroscopy with Photoelectrons": K. Müller-Dethlefs in reference [19], p. 21.
[21] K. Müller-Dethlefs, E. W. Schlag, E. Grant, K. Wang, B. V. McKoy, *Adv. Chem. Phys.* **1995**, *90*, 1.
[22] F. Merkt, T. Softley, *Int. Rev. Phys. Chem.* **1993**, *12*, 205.
[23] H.-J. Dietrich, K. Müller-Dethlefs, L. Y. Baranov, *Phys. Rev. Lett.* **1996**, *76*, 3530.
[24] H.-J. Dietrich, R. Lindner, K. Müller-Dethlefs, *J. Chem. Phys.* **1994**, *101*, 3399.
[25] R. Lindner, H.-J. Dietrich, K. Müller-Dethlefs, *Chem. Phys. Lett.* **1994**, *228*, 417.
[26] E. R. Grant, M. G. White, *Nature* **1991**, *354*, 249.
[27] K. Wang, V. McKoy, *Annu. Rev. Phys. Chem.* **1995**, *46*, 275.
[28] G. Reiser, W. Habenicht, K. Müller-Dethlefs, E. W. Schlag, *Chem. Phys. Lett.* **1988**, *152*, 119.
[29] K. Müller-Dethlefs, W. A. Chupka, E. Eyler, S. D. Colson, private symposium, Yale, **1988**.
[30] W. A. Chupka, personal communication, **1988**.
[31] W. A. Chupka, *J. Chem. Phys.* **1993**, *98*, 4520; *ibid.* **1993**, *99*, 5800.
[32] R. Lindner, H. Sekiya, K. Müller-Dethlefs, *Angew. Chem.* **1993**, *105*, 1384; *Angew. Chem. Int. Ed. Engl.* **1993**, *32*, 1364; R. Lindner, B. Beyl, H. Sekiya, K. Müller-Dethlefs, *ibid.* **1993**, *105*, 631 and **1993**, *32*, 603.
[33] G. Reiser, D. Rieger, T. G. Wright, K. Müller-Dethlefs, E. W. Schlag, *J. Phys. Chem.* **1993**, *97*, 4335.
[34] E. Sekreta, K. S. Visvanathan, J. P. Reilly, *J. Chem. Phys.* **1989**, *90*, 5349.
[35] I. Fischer, A. Strobel, J. Staeker, G. Niedner-Schatteburg, K. Müller-Dethlefs, V. E. Bondybey, *J. Chem. Phys.* **1992**, *96*, 7171.
[36] T. Vondrak, S. Sato, K. Kimura, *J. Phys. Chem. A* **1997**, *101*, 2384.
[37] D. A. Rodham, G. A. Blake, *Chem. Phys. Lett.* **1997**, *264*, 522.
[38] T. Kitsopoulos, C. J. Chick, Y. Zhao, D. M. Neumark, *J. Chem. Phys.* **1991**, *95*, 1441.
[39] G. Ganteför, D. M. Cox, A. Kaldor, *J. Chem. Phys.* **1990**, *93*, 8395.
[40] G. Reiser, O. Dopfer, R. Lindner, G. Henri, K. Müller-Dethlefs, E. W. Schlag, S. D. Colson, *Chem. Phys. Lett.* **1991**, *181*, 1.
[41] O. Dopfer, G. Reiser, K. Müller-Dethlefs, *Ber. Bunsen-Ges. Phys. Chem.* **1992**, *96*, 1259.
[42] O. Dopfer, G. Reiser, K. Müller-Dethlefs, E. W. Schlag, S. D. Colson, *J. Chem. Phys.* **1994**, *101*, 974.
[43] T. G. Wright, E. Cordes, O. Dopfer, K. Müller-Dethlefs, *J. Chem. Soc. Faraday Trans.* **1993**, *89*, 1609.
[44] E. Cordes, O. Dopfer, T. G. Wright, K. Müller-Dethlefs, *J. Phys. Chem.* **1993**, *97*, 7471.
[45] O. Dopfer, G. Lembach, T. G. Wright, K. Müller-Dethlefs, *J. Chem. Phys.* **1993**, *98*, 1933.
[46] T. G. Wright, O. Dopfer, E. Cordes, K. Müller-Dethlefs, *J. Am. Chem. Soc.* **1994**, *116*, 5880.
[47] W. Habenicht, G. Reiser, K. Müller-Dethlefs, *J. Chem. Phys.* **1991**, *95*, 4809.
[48] K. Müller-Dethlefs, *J. Chem. Phys.* **1991**, *95*, 4821.
[49] W. B. Peatman, T. B. Borne, E. W. Schlag, *Chem. Phys. Lett.* **1969**, *3*, 492.

[50] E. Waterstradt, H.-J. Dietrich, K. Müller-Dethlefs, *Rev. Sci. Instrum.* **1993**, *94*, 3104.
[51] K. Müller-Dethlefs, *J. Electron Spectrosc. Relat. Phenom.* **1995**, *75*, 35.
[52] H. Sekiya, R. Lindner, K. Müller-Dethlefs, *Chem. Lett.* **1993**, 485.
[53] R. Lindner, K. Müller-Dethlefs, E. Wedom, K. Haber, E. R. Grant, *Science* **1996**, *271*, 1698.
[54] R. Lindner, H. Sekiya, K. Müller-Dethlefs, *J. Chem. Phys.*, submitted.
[55] L. Y. Baranov, R. Kris, R. D. Levine, U. Even, *J. Chem. Phys.* **1994**, *100*, 186.
[56] J. Jortner, M. Bixon, *J. Chem. Phys.* **1995**, *102*, 5636.
[57] M. Bixon, J. Jortner, *J. Chem. Phys.* **1995**, *103*, 4431.
[58] M. Bixon, J. Jortner, *Mol. Phys.* **1996**, *89*, 373.
[59] E. Rabani, R. D. Levine, *J. Chem. Phys.* **1996**, *104*, 1937.
[60] D. Bahatt, U. Even, R. D. Levine, *J. Chem. Phys.* **1993**, *98*, 1744.
[61] U. Even, M. Ben-Nun, R. D. Levine, *Chem. Phys. Lett.* **1993**, *210*, 416.
[62] F. Merkt, R. N. Zare, *J. Chem. Phys.* **1994**, *101*, 3495.
[63] F. Merkt, H. Xu, R. N. Zare, *J. Chem. Phys.* **1996**, *104*, 950.
[64] T. N. Kitsopoulos, I. M. Waller, J. G. Loeser, D. M. Neumark, *Chem. Phys. Lett.* **1989**, *159*, 300.
[65] I. M. Waller, T. N. Kitsopoulos, D. M. Neumark, *J. Phys. Chem.* **1990**, *94*, 2240.
[66] D. M. Neumark, *Annu. Rev. Phys. Chem.* **1992**, *43*, 153; R. B. Metz, S. E. Bradforth, D. M. Neumark, *Adv. Chem. Phys.* **1992**, *81*, 1.
[67] G. Herzberg, *Molecular Spectra and Molecular Structure*, *Vol. I*, *Spectra of Diatomic Molecules*, Van Nostrand, Princeton, **1950**.
[68] H. Rudolph, V. McKoy, S. N. Dixit, *J. Chem. Phys.* **1989**, *90*, 2570.
[69] M. Sander, L. A. Chewter, K. Müller-Dethlefs, E. W. Schlag, *Phys. Rev. A* **1987**, *36*, 4543.
[70] I. Fischer, A. Lochschmidt, A. Strobel, G. Niedner-Schatteburg, K. Müller-Dethlefs, V. E. Bondybey, *J. Chem. Phys.* **1993**, *98*, 3592.
[71] S. R. Mackenzie, E. J. Halse, E. Gordon, D. Rolland, T. P. Softley, *Chem. Phys. Lett.* **1996**, *209*, 127.
[72] M. C. R. Cockett, J. G. Goode, K. P. Lawley, R. J. Donovan, *J. Chem. Phys.* **1995**, *102*, 5226.
[73] M. C. R. Cockett, *J. Phys. Chem.* **1995**, *99*, 16228.
[74] M. C. R. Cockett, J. G. Goode, R. J. Maier, K. P. Lawley, R. J. Donovan, *J. Chem. Phys.* **1994**, *101*, 126.
[75] R. J. Donovan, A. C. Fleten, K. P. Lawley, T. Ridley, *Chem. Phys.* **1997**, *226*, 217.
[76] A. Strobel, I. Fischer, A. Lochschmidt, K. Müller-Dethlefs, V. E. Bondybey, *J. Phys. Chem.* **1994**, *98*, 2024.
[77] J. W. Hepburn, *Chem. Soc. Rev.* **1996**, *25*, 281.
[78] A. Wills, D. Cubric, M. Ukai, F. Currell, B. J. Goodwin, T. Reddish, J. Comer, *J. Phys. B* **1993**, *26*, 2601.
[79] M. Bixon, J. Jortner, *J. Chem. Phys.* **1996**, *105*, 1363.
[80] A. Wills, A. A. Cafolla, J. Comer, *J. Phys. B* **1991**, *24*, 3939.
[81] P. Morin, I. Nenner, *Phys. Rev. Lett.* **1986**, *56*, 1913.
[82] A. Mank, T. Nguyen, J. D. D. Martin, J. W. Hepburn, *Phys. Rev. A* **1995**, *51*, R1.
[83] L. A. Chewter, M. Sander, K. Müller-Dethlefs, E. W. Schlag, *J. Chem. Phys.* **1987**, *86*, 4737.
[84] The $\tilde{X}^+$ label is often used in place of D_0 for polyatomic molecules in this article to refer to the cation ground state.
[85] S. T. Pratt, P. M. Dehmer, J. L. Dehmer, *J. Chem. Phys.* **1993**, *99*, 6233.
[86] J. K. G. Watson, M. Herman, J. C. van Craen, R. Colin, *J. Mol. Spectrosc.* **1982**, *95*, 101.
[87] J. C. van Craen, M. Herman, R. Colin, J. K. G. Watson, *J. Mol. Spectrosc.* **1985**, *111*, 185.
[88] F. Merkt, S. R. Mackenzie, R. J. Rednall, T. P. Softley, *J. Chem. Phys.* **1993**, *99*, 8430.
[89] A. D. Buckingham, B. J. Orr, J. M. Sichel, *Philos. Trans. R. Soc. London A* **1970**, *268*, 147.
[90] C. Cossart-Magos, M. Jungen, F. Lawney, *Mol. Phys.* **1987**, *61*, 1077.
[91] J. H. Callomon, T. M. Dunn, I. M. Mills, *Philos. Trans. R. Soc. London A* **1966**, *259*, 499.
[92] M. Oldani, R. Widmer, G. Grassi, A. Bauder, *J. Mol. Struct.* **1988**, *190*, 31.
[93] E. Riedle, T. Knittel, T. Weber, H. J. Neusser, *J. Chem. Phys.* **1989**, *91*, 4555.
[94] E. Riedle, J. Pliva, *Chem. Phys.* **1991**, *152*, 375.
[95] H. A. Jahn, E. Teller, *Proc. R. Soc. London A* **1937**, *161*, 220.
[96] U. Öpik, M. H. L. Pryce, *Proc. R. Soc. London A* **1956**, *238*, 425.
[97] I. B. Bersuker, *The Jahn-Teller Effect and Vibronic Interactions in Modern Chemistry*, Plenum, New York, **1984**.
[98] K. Raghavachari, R. C. Haddon, T. A. Miller, V. E. Bondybey, *J. Chem. Phys.* **1983**, *79*, 1387.
[99] T. A. Miller, V. E. Bondybey, *Molecular Ions: Spectroscopy*, *Structure and Chemistry*, North Holland, Amsterdam, **1983**.
[100] M. Iwasaki, K. Toriyama, K. Nunome, *J. Chem. Soc. Chem. Commun.* **1983**, 320.
[101] S. R. Long, J. T. Meek, J. P. Reilly, *J. Chem. Phys.* **1983**, *79*, 3206.
[102] P. R. Bunker, *Molecular Symmetry and Spectroscopy*, Academic Press, New York, **1979**.
[103] E. B. Wilson, *Phys. Rev.* **1934**, *45*, 706.
[104] H. C. Longuet-Higgins, U. Öpik, M. H. L. Pryce, F. R. S. Sack, R. A. Sack, *Proc. R. Soc. London A* **1958**, *244*, 1; R. L. Whetten, K. S. Haber, E. R. Grant, *J. Chem. Phys.* **1986**, *84*, 1270.
[105] J. Eiding, W. Domcke, *Chem. Phys.* **1992**, *163*, 133.
[106] W. von Niessen, G. H. F. Diercksen, L. S. Cederbaum, *Chem. Phys. Lett.* **1977**, *45*, 295.
[107] M. H. Palmer, W. Moyes, M. Spiers, J. N. A. Ridyard, *J. Mol. Struct.* **1978**, *49*, 105.
[108] G. Bieri, L. Åsbrink, W. von Niessen, *J. Electron Spectrosc. Relat. Phenom.* **1981**, *23*, 281.
[109] X. Song, C. W. Wilkerson, J. Lucia, S. Pauls, J. P. Reilly, *Chem. Phys. Lett.* **1990**, *174*, 377.
[110] S. Hillenbrand, L. Zhu, P. Johnson, *J. Chem. Phys.* **1991**, *95*, 2237.
[111] K.-T. Lu, G. C. Eiden, J. C. Weisshaar, *J. Phys. Chem.* **1992**, *96*, 9742.
[112] K. Okuyama, M. R. C. Cockett, K. Kimura, *J. Chem. Phys.* **1992**, *97*, 1649.
[113] G. C. Eiden, F. Weinhold, J. C. Weisshaar, *J. Chem. Phys.* **1991**, *95*, 8665.
[114] J. A. Blush, P. Chen, R. T. Wiedmann, M. G. White, *J. Chem. Phys.* **1993**, *98*, 3557.
[115] P. Hobza, R. Zahradník, *Intermolecular Complexes: The Role of van der Waals Systems in Physical Chemistry and in the Biodisciplines*, Elsevier, Amsterdam, **1988**.
[116] M. Ito, *J. Mol. Struct.* **1988**, *177*, 173.
[117] M. Ito in *Vibrational Spectra and Structure*, *Vol. 15* (Ed.: J. R. Durig), Elsevier, Amsterdam, **1986**; M. Ito, T. Ebata, N. Mikami, *Annu. Rev. Phys. Chem.* **1988**, *39*, 123; M. Ito, S. Yamamoto, T. Aoto, T. Ebata, *J. Mol. Struct.* **1990**, *237*, 105; M. Gerhards, B. Kimpfel, M. Pohl, M. Schmitt, K. Kleinermanns, *J. Mol. Struct.* **1992**, *270*, 301.
[118] T. Oka, *Rev. Mod. Phys.* **1992**, *64*, 1141.
[119] E. Hirota, *Chem. Rev.* **1992**, *92*, 141.
[120] C. G. Bailey, J. Kim, C. E. H. Dessent, M. A. Johnson, *Chem. Phys. Lett.* **1997**, *269*, 122.
[121] O. Dopfer, K. Müller-Dethlefs, *J. Chem. Phys.* **1994**, *101*, 8508.
[122] M. Schütz, T. Bürgi, S. Leutwyler, T. Fischer, *J. Chem. Phys.* **1993**, *98*, 3763.
[123] M. Schütz, T. Bürgi, S. Leutwyler, *J. Mol. Struct.* **1992**, *276*, 117.
[124] D. Feller, M. W. Feyereisen, *J. Comput. Chem.* **1993**, *14*, 1027.
[125] P. Hobza, R. Burcl, V. Spirko, O. Dopfer, K. Müller-Dethlefs, E. W. Schlag, *J. Chem. Phys.* **1994**, *101*, 990.
[126] R. J. Lipert, S. D. Colson, *J. Phys. Chem.* **1989**, *93*, 135.
[127] K. Fuke, H. Yoshiuchi, K. Kaya, Y. Achiba, K. Sato, K. Kimura, *Chem. Phys. Lett.* **1984**, *108*, 179.
[128] R. J. Lipert, S. D. Colson, *J. Chem. Phys.* **1988**, *89*, 4579.
[129] G. Lembach, Diplomarbeit, Technische Universität München, **1992**.
[130] O. Dopfer, Dissertation, Technische Universität München, **1994**.
[131] For the hydrogen-bonded complexes PhOH – MeOH, PhOH – EtOH, PhOH – DME, and PhOH – PhOH the following nomenclature is used for the six intermolecular vibrations: ξ_i for bendings and the torsion ($i = 1-5$) and σ for the stretching vibration in the S_1 state; η_i for bendings and the torsion ($i = 1-5$) and σ_+ for the stretching vibration in the ionic ground state
[132] H. Abe, N. Mikami, M. Ito, Y. Udagawa, *J. Phys. Chem.* **1982**, *86*, 2567.
[133] L. A. Chewter, K. Müller-Dethlefs, E. W. Schlag, *Chem. Phys. Lett.* **1987**, *135*, 219.
[134] X. Zhang, J. M. Smith, J. L. Knee, *J. Chem. Phys.* **1992**, *97*, 2843.

[135] E. J. Bieske, A. Z. Vichanco, M. W. Rainbird, A. E. W. Knight, *J. Chem. Phys.* **1991**, *94*, 7029.
[136] X. Zhang, J. L. Knee, *Faraday Discuss. Chem. Soc.* **1994**, *97*, 299.
[137] L. Zhu, P. M. Johnson, *J. Chem. Phys.* **1991**, *94*, 5769.
[138] H. Krause, H. J. Neusser, *J. Chem. Phys.* **1992**, *97*, 5923.
[139] T. L. Grebner, P. V. Unold, H. J. Neusser, *J. Phys. Chem. A* **1997**, *101*, 158.
[140] G. Lembach, B. Brutschy, *J. Phys. Chem*. **1996**, *100*, 19758.
[141] H. J. Neusser, H. Krause, *Int. J. Mass Spectrom. Ion Processes* **1994**, *131*, 211.
[142] T. L. Grebner, Dissertation, Technische Universität München, **1996**.
[143] W. G. Scherzer, H. L. Selzle, E. W. Schlag, *Z. Naturforsch. A* **1993**, *48*, 1256.
[144] C. Alt, W. G. Scherzer, H. L. Selzle, E. W. Schlag, *Chem. Phys. Lett.* **1995**, *240*, 457.
[145] W. G. Scherzer, H. L. Selzle, E. W. Schlag, R. D. Levine, *Phys. Rev. Lett*. **1994**, *72*, 1435.
[146] O. Dopfer, M. Melf, K. Müller-Dethlefs, *Chem. Phys.* **1996**, *207*, 437.
[147] G. I. Németh, H. Ungar, C. Yeretzian, H. L. Selzle, E. W. Schlag, *Chem. Phys. Lett.* **1994**, *228*, 1.
[148] C. Yeretzian, R. H. Hermann, H. Ungar, H. L. Selzle, E. W. Schlag, S. H. Lin, *Chem. Phys. Lett.* **1995**, *239*, 61.
[149] D. S. Yang, A. M. James, D. M. Rayner, P. A. Hackett, *Chem. Phys. Lett.* **1994**, *231*, 177.
[150] D. S. Yang, A. M. James, D. M. Rayner, P. A. Hackett, *J. Chem. Phys.* **1995**, *102*, 3129.
[151] D. S. Yang, M. Z. Zgierski, D. M. Rayner, P. A. Hackett, A. Martinez, D. R. Salahub, P.-N. Roy, T. Carrington, *J. Chem. Phys.* **1995**, *103*, 5335.
[152] D. S. Yang, M. Z. Zgierski, A. Bérces, P. A. Hackett, P.-N. Roy, A. Martinez, T. Carrington, D. R. Salahub, R. Fournier, T. Pang, C. Chen, *J. Chem. Phys.* **1996**, *105*, 10663.
[153] K. Müller-Dethlefs, M. Cockett in *Nonlinear Spectroscopy for Molecular Structure Determination* (Eds.: R. W. Field, E. Hirota, J. P. Maier, S. Tsuchiya), Blackwell Science, Oxford, **1998**, p. 167 ff.
[154] G. Burton, C. Xu, C. C. Arnold, D. M. Neumark, *J. Chem. Phys.* **1996**, *104*, 2757.
[155] C. C. Arnold, D. M. Neumark, *J. Chem. Phys.* **1994**, *100*, 1779.
[156] C. C. Arnold, D. M. Neumark, D. M. Cyr, M. A. Johnson, *J. Phys. Chem.* **1995**, *99*, 1633.
[157] Y. Zhao, C. C. Arnold, D. M. Neumark, *Faraday Discuss. Chem. Soc.* **1993**, *89*, 1449.
[158] C. Bässmann, U. Boesl, D. Yang, G. Drechsler, E. W. Schlag, *Int. J. Mass Spectrom. Ion Processes* **1996**, *159*, 153.
[159] C. E. H. Dessent, C. G. Bailey, M. A. Johnson, *J. Chem. Phys.* **1995**, *102*, 6336; *ibid.* **1995**, *103*, 2006; D. Serxner, C. E. H. Dessent, M. A. Johnson, *ibid*. **1996**, *105*, 7231.
[160] M. A. Johnson, personal communication.
[161] C. E. H. Dessent, J. Kim, M. A. Johnson, *Acc. Chem. Res.*, in press.
[162] G. F. Ganteför, D. M. Cox, A. Kaldor, *Z. Phys. D* **1991**, *19*, 59.
[163] G. F. Ganteför, D. M. Cox, A. Kaldor, *J. Chem. Phys.* **1992**, *96*, 4102.
[164] G. Drechsler, C. Bässmann, U. Boesl, E. W. Schlag, *Z. Naturforsch. A* **1994**, *49*, 1256.
[165] G. Drechsler, C. Bässmann, U. Boesl, E. W. Schlag, *J. Mol. Struct.* **1995**, *348*, 337.
[166] Reviews: D. M. Neumark, *Annu. Rev. Phys. Chem.* **1992**, *43*, 153; R. B. Metz, S. E. Bradforth, D. M. Neumark, *Adv. Chem. Phys.* **1992**, *81*, 1; D. M. Neumark, *Acc. Chem. Res.* **1993**, *26*, 33.
[167] R. B. Metz, T. N. Kitsopoulos, A. Weaver, D. M. Neumark, *J. Chem. Phys.* **1988**, *88*, 1463.
[168] A. Weaver, R. B. Metz, S. E. Bradforth, D. M. Neumark, *J. Phys. Chem.* **1988**, *92*, 5558.
[169] R. B. Metz, A. Weaver, S. E. Bradforth, T. N. Kitsopoulos, D. M. Neumark, *J. Phys. Chem.* **1990**, *94*, 1377.
[170] A. Weaver, D. M. Neumark, *Faraday Discuss. Chem. Soc.* **1991**, *91*, 5; S. E. Bradforth, D. W. Arnold, D. M. Neumark, D. E. Manolopoulos, *J. Chem. Phys.* **1993**, *99*, 6345.
[171] N. E. Klepeis, A. L. L. East, A. G. Császár, W. D. Allen, T. J. Lee, D. W. Schwenke, *J. Chem. Phys.* **1993**, *99*, 3865.
[172] G. C. Schatz, S. Florance, T. J. Lee, C. W. Bauschlicher, Jr., *Chem. Phys. Lett.* **1993**, *202*, 495.
[173] C. M. Ellison, B. S. Ault, *J. Phys. Chem.* **1979**, *83*, 832.
[174] See literature cited in reference [168].
[175] R. B. Metz, D. M. Neumark, *J. Chem. Phys.* **1992**, *97*, 962.
[176] S. P. Walch, C. W. Bauschlicher, Jr., S. R. Langhoff, *J. Chem. Phys.* **1986**, *85*, 5900.
[177] C. M. Rohfing, K. Raghavachari, *J. Chem. Phys.* **1992**, *96*, 2114.
[178] D. A. Dixon, J. L. Gole, *Chem. Phys. Lett.* **1992**, *188*, 560; R. Fournier, S. B. Sinnott, A. DePristo, *J. Chem. Phys.* **1992**, *97*, 4149.
[179] C. C. Arnold, D. M. Neumark, *J. Chem. Phys.* **1993**, 99, 3353.
[180] J. A. Syage, J. Steadman, *J. Chem. Phys.* **1991**, *95*, 2497; J. A. Syage, *J. Phys. Chem.* **1993**, *97*, 12523.
[181] F. Remacle, U. Even, R. D. Levine, *J. Phys. Chem.* **1996**, *100*, 19735.
[182] A. Mühlpfordt, U. Even, E. P. Ernsting, *Chem. Phys. Lett.* **1996**, *263*, 178.